

Dielectronic Recombination Lines of C⁺

Taha Sochi^{a,1,*}, Peter J. Storey^{a,1,1}

^a*University College London, Department of Physics and Astronomy, Gower Street, London, WC1E 6BT*

Abstract

The current paper presents atomic data generated to investigate the recombination lines of C II in the spectra of planetary nebulae. These data include energies of bound and autoionizing states, oscillator strengths and radiative transition probabilities, autoionization probabilities, and recombination coefficients. The R-matrix method of electron scattering theory was used to describe the C²⁺ plus electron system.

Keywords: C II spectra; atomic spectroscopy; dielectronic recombination; oscillator strength; bound state; resonance.

arXiv:1212.6083v1 [physics.atom-ph] 25 Dec 2012

*Corresponding author.

Email address: E-mail: t.sochi@ucl.ac.uk (Taha Sochi)

Contents

1. Introduction	3
2. Tools and Methods of Calculation	4
2.1. Autoionizing and Bound States Calculations	4
2.2. Oscillator Strength Calculations	6
2.3. Emissivity Calculations	7
3. Comparison to Previous Work	8
4. Results	8
5. Conclusions	9
References	10

Tables

1. The available experimental data from NIST for the bound states of C^+ below the $C^{2+} 1S_0^e$ threshold alongside the theoretical results from R -matrix calculations.	21
2. The available experimental data from NIST for the resonance states of C^+ above the $C^{2+} 1S_0^e$ threshold alongside the theoretical results as obtained by K -matrix and QB methods.	25
3. Free-bound f -values for bound symmetry $J^\pi = 1/2^o$ obtained by integrating photoionization cross sections from R -matrix calculations. The superscript denotes the power of 10 by which the number is to be multiplied.	27
4. Free-bound f -values for bound symmetry $J^\pi = 3/2^o$ obtained by integrating photoionization cross sections from R -matrix calculations. The superscript denotes the power of 10 by which the number is to be multiplied.	28
5. Free-bound f -values for bound symmetry $J^\pi = 5/2^o$ obtained by integrating photoionization cross sections from R -matrix calculations. The superscript denotes the power of 10 by which the number is to be multiplied.	29
6. Sample of our line list where several lines have been observed astronomically. The first column is for experimental/theoretical energy identification for the upper and lower states respectively where 1 refers to experimental while 0 refers to theoretical. The other columns are for the atomic designation of the upper and lower states respectively, followed by the air wavelength in angstrom and effective dielectronic recombination rate coefficients in $cm^3.s^{-1}$ for the given logarithmic temperatures. The superscript denotes the power of 10 by which the number is to be multiplied.	30

1. Introduction

The study of atomic and ionic lines of carbon in the spectra of astronomical objects, such as planetary nebulae [1–3], has implications for carbon abundance determination [4–9], probing the physical conditions in the interstellar medium [10, 11], and element enrichment in the CNO cycle [7, 12, 13]. The lines span large parts of the electromagnetic spectrum and originate from various processes under different physical conditions. Concerning C^+ , the subject of the current investigation, spectral lines have been observed in many astronomical objects such as planetary nebulae, Seyfert galaxies, stellar winds of Wolf-Rayet stars, symbiotic stars, and in the interstellar medium [8, 12, 14–19].

Many atomic processes can contribute to the production of carbon spectral lines, including radiative and collisional excitation, and radiative and dielectronic recombination. The current study is concerned with some of the lines produced by dielectronic recombination and subsequent radiative cascades.

Capture of an incoming electron to a target ion may occur through a non-resonant background continuum, which is radiative recombination (RR), or through a process involving doubly-excited states (resonances) known as dielectronic recombination (DR). The latter can lead either to autoionization, a radiationless transition to a lower state of the ion with the ejection of a free electron, or to stabilization by radiative decay to a lower true bound state.

The rate for RR rises as the free electron temperature falls and hence tends to be the dominant recombination process at low temperatures. It is particularly significant in the cold ionized plasmas found, for example, in some supernova remnants [20–22].

We may distinguish three types of DR mechanism with relevance at different temperatures

1. High-temperature DR (HTDR) which occurs through Rydberg series of autoionizing states, and in which the radiative stabilization is via a decay within the ion core.
2. Low-temperature DR (LTDR) which operates via a few near-threshold resonances with radiative stabilization usually through decay of the outer, captured electron. These resonances are usually within a few thousand wave numbers of threshold, so this process operates at thousands to tens of thousands of degrees Kelvin.
3. Fine-structure DR (FSDR) which is due to Rydberg series resonances converging on the fine-structure levels of the ground term of the recombining ion, and is necessarily stabilized by outer electron decays. This process can operate at very low temperatures, down to tens or hundreds of Kelvin.

In this paper we are concerned only with LTDR and the resulting spectral lines.

With regard to the recombination lines of $C\ II$, there are many theoretical and observational studies mainly within astronomical contexts. Examples are [5, 6, 9–12, 15–18, 20, 23–34]. From the perspective of atomic physics, the most comprehensive of these studies and most relevant to the current investigation is that of Badnell [31] who calculated configuration mixing effective dielectronic recombination coefficients for the recombined C^+ ion at temperatures $T = 10^3 - 6.3 \times 10^4$ K applicable to planetary nebulae, and Davey *et al* [16] who computed effective recombination coefficients for $C\ II$ transitions between doublet states for the temperature range 500–20000 K with an electron density of 10^4 cm^{-3} relevant to planetary nebulae. Badnell performed calculations in both LS and intermediate coupling schemes and over a wide temperature range, using the Autostructure code which treats the autoionizing states as bound and the interaction with continuum states by a perturbative approach. On the other hand, Davey *et al* performed their calculations using

the **R**-matrix code which uses a unified treatment of bound and continuum states but worked in the LS -coupling scheme and hence their results were limited to doublet states.

The aim of the current study is to treat the near-threshold resonances and subsequent radiative decays using the unified approach of the **R**-matrix method in intermediate coupling. The investigation includes all the autoionizing resonance states above the threshold of $C^{2+} 1S^e$ with a principal quantum number $n < 5$ for the captured electron as an upper limit. This condition was adopted mainly due to computational limitations. In total, 61 autoionizing states (27 doublets and 34 quartets) with this condition have been theoretically found by the **R**-matrix method. Of these 61 resonances, 55 are experimentally observed according to the NIST database [35]. More details will follow in the forthcoming sections.

2. Tools and Methods of Calculation

2.1. Autoionizing and Bound States Calculations

We use the **R**-matrix code [36], and Autostructure [37–39] to compute the properties of autoionizing and bound states of C^+ . Orbitals describing the target for the **R**-matrix scattering calculations were taken from Berrington *et al* [40], who used a target comprising the six terms $2s^2 1S^e$, $2s2p 3P^o$, $1P^o$ and $2p^2 3P^e$, $1D^e$, $1S^e$, constructed from seven orthogonal orbitals; three physical and four pseudo orbitals. These orbitals are: $1s$, $2s$, $2p$, $\bar{3}s$, $\bar{3}p$, $\bar{3}d$ and $\bar{4}f$, where the bar denotes a pseudo orbital. The purpose of including pseudo orbitals is to represent electron correlation effects and to improve the target wavefunctions. The radial parts, $P_{nl}(r)$, of these orbitals are Slater Type Orbital (STO) generated by the CIV3 program of Hibbert [41]. Each STO is defined by

$$P_{nl}(r) = \sum_i C_i r^{P_i} e^{-\xi_i r} \quad (1)$$

where C_i is a coefficient and P_i and ξ_i are indicial parameters in this specification, r is the radius, and i is a counting index that runs over the orbitals of interest. The values of these parameters are given in Table (A).

In this work we construct a scattering target of 26 terms which includes the 6 terms of Berrington *et al* [40] plus all terms of the configurations $2s\bar{3}l$ and $2p\bar{3}l$, $l=0, 1, 2$. This includes the terms outside the $n=2$ complex which make the largest contribution to the dipole polarizability of the $2s^2 1S^e$ and $2s2p 3P^o$ states of C^{2+} .

The **R**-matrix calculations were carried out in the intermediate coupling (IC) scheme by including the spin-orbit interaction terms of the Breit-Pauli Hamiltonian. The requirement for the IC scheme arises from the fact that in LS -coupling the conserved quantities are $LS\pi$ and hence only the doublet states that conserve these quantities, such as $2S^e$ and $2P^o$, can autoionize. Therefore, in LS -coupling no autoionization is allowed for quartet terms or some doublet states, such as $2S^o$ and $2P^e$.

The number of continuum basis orbitals used to express the wavefunction in the inner region (MAXC in STG1 of the **R**-matrix code) was varied between 6-41 and the results were analyzed. It was noticed that increasing the number of basis functions, with all ensuing computational costs, does not necessarily improve the results; moreover a convergence instability may occur in some cases. It was decided therefore to use MAXC = 16 in all calculations as a compromise between the computational resources requirement and accuracy. The effect of varying the size of the inner region radius in the **R**-matrix formulation was also investigated and a value of 10 atomic units was chosen on the basis of numerical stability and convergence.

Several methods exist for finding and analyzing resonances that arise during the recombination processes; these methods include the Time-Delay method of Stibbe and Tennyson [42] which is based on the use of lifetime matrix eigenvalues [43] to locate the resonance position and identify its width, and the **QB** method of Quigley *et al* [44, 45] which applies a fitting procedure to the reactance matrix eigenphase near the resonance position using the analytic properties of the **R**-matrix theory.

For the low-lying resonances just above the $^1\text{S}^e$ ionization threshold, the scattering matrix **S** has only one channel, and hence the reactance matrix, **K**, is a real scalar with a pole near the resonance position. According to the collision theory of Smith [43], the lifetime matrix **M** is related to the **S**-matrix by

$$\mathbf{M} = -i\hbar\mathbf{S}^*\frac{d\mathbf{S}}{dE} \quad (2)$$

where i is the imaginary unit, \hbar ($= h/2\pi$) is the reduced Planck's constant, \mathbf{S}^* is the complex conjugate of **S**, and E is the energy. Now, a **K**-matrix with a pole at energy E_0 superimposed on a background K_o can be approximated by

$$K_i = K_o + \frac{g}{E_i - E_0} \quad (3)$$

where K_i is the value of **K**-matrix at energy E_i and g is a physical parameter with dimension of energy. It follows that in the case of single-channel scattering the **M**-matrix is real with a value given by

$$M = \frac{-2g}{(1 + K_o^2)(E - E_0)^2 + 2K_o g(E - E_0) + g^2} \quad (4)$$

Using the fact demonstrated by Smith [43] that the lifetime of the state is the expectation value of M , it can be shown from Equation (4) that the position of the resonance peak E_r is given by

$$E_r = E_0 - \frac{K_o g}{1 + K_o^2} \quad (5)$$

while the full width at half maximum Δ_E is given by

$$\Delta_E = \frac{|2g|}{1 + K_o^2} \quad (6)$$

The two parameters of primary interest to our investigation are the resonance energy position E_r , and the resonance width Δ_r which equals the full width at half maximum Δ_E . However, for an energy point E_i with a **K**-matrix value K_i , Equation (3) has three unknowns, K_o , g and E_0 , which are needed to find E_r and Δ_r . Hence, three energy points in the immediate neighborhood of E_0 are required to identify these unknowns. As the **K**-matrix changes sign at the pole, the neighborhood of E_0 is located by testing the **K**-matrix value at each point of the energy mesh for sign change. Consequently, the three points are obtained and can be used to find E_r and Δ_r .

To improve the performance of this approach, an interactive graphical technique was developed to read and plot the **K**-matrix data directly while searching for poles. In a later stage, more efficient non-graphical tools for pole searching were used. The purpose of these tools is to search for any sudden increase or decrease in the background of the **K**-matrix where poles do exist and where a search with a finer energy mesh would then be carried out.

With regard to sampling the three points for the **K**-matrix calculations, it was observed that sampling the points very close to the pole makes the energy position and width of resonances susceptible to fluctuations and instabilities. Therefore, a sampling scheme was adopted in which the points are selected from a broad range not too close to the pole.

This approach was implemented by generating two meshes, coarse and fine, around the pole as soon as the pole is found. To check the results, several different three-point combinations for each resonance were used to find the position and width of the resonance. In each case, the results from these different combinations were compared. In all cases they were identical within acceptable numerical errors. The results of **QB** confirm this conclusion as they agree with the **K**-matrix results as can be seen in Table (2).

The results for all bound and autoionizing states are given in Tables (1-2). In total, 142 bound states belonging to 11 symmetries ($2J = 1, 3, 5, 7, 9$ even and $2J = 1, 3, 5, 7, 9, 11$ odd) and 61 resonances belonging to 11 symmetries ($2J = 1, 3, 5, 7, 9, 11$ even and $2J = 1, 3, 5, 7, 9$ odd) were identified. As seen in Tables (1-2), the theoretical results for both bound and resonance states agree very well with the available experimental data both in energy levels and in fine structure splitting. Experimental energies are not available for the very broad resonances as they are difficult to find experimentally. The maximum discrepancy between experiment and theory in the worst case does not exceed a few percent. Furthermore, the ordering of the energy levels is the same between the theoretical and experimental in most cases. Order reversal in some cases is indicated by a minus sign in the fine structure splitting.

2.2. Oscillator Strength Calculations

The oscillator strengths for free-free, free-bound and bound-bound transitions are required to find the radiative probabilities for these transitions. As there is no free-free stage in the available **R**-matrix code, the f -values for the free-free transitions could not be produced by **R**-matrix. Therefore, these values were generated by Autostructure in the intermediate coupling scheme where 60 electron configurations were included in the Autostructure input: $2s^2 nl$ ($2p \leq nl \leq 7s$), $2s2p nl$ ($2p \leq nl \leq 7s$), $2p^3$, and $2p^2 nl$ ($3s \leq nl \leq 7s$). An iterative procedure was followed to find the orbital scaling parameters (λ 's) required in Autostructure. These parameters are given in Table (B). The scaling parameters, which are obtained by Autostructure in an automated optimization variational process, are required to minimize the weighted energy sum of the included target states [37, 46, 47].

Regarding the free-bound transitions, the f -values for more than 2500 free-bound transitions were computed by integrating the photoionization cross sections (in mega barn) over the photon energy (in Rydberg). This was done for each bound state and for all resonances in the corresponding cross-section. The area under the cross-section curve comprises a background contribution, assumed linear with energy, and the contribution due to the resonance, which is directly related to the bound-free oscillator strength. The photoionization cross sections as a function of photon energy were generated by stage STGBF of the **R**-matrix code. Some representative cross-sections are shown in Figure (1) which displays a number of examples of photoionization cross sections of the indicated bound states close to the designated autoionizing states. It should be remarked that a separate energy mesh was used to generate photoionization cross section data for each individual resonance with a refinement process to ensure correct mapping and to avoid peak overlapping from different resonances.

The f -values of the bound-bound transitions were calculated using stage STGGB of the **R**-matrix code. However, the bound-bound f -values for the 8 uppermost bound states, namely the $2s2p(^3P^o)3d\ ^4F^o$ and $^4D^o$ levels, were generated by Autostructure using similar input data and procedures to those used in generating the f -values for the free-free transitions, as outlined earlier. These states have very large effective quantum number and hence are out of validity range of the **R**-matrix code. Autostructure was also used to generate the free-bound f -values for these 8 uppermost

bound states for the same reason.

2.3. Emissivity Calculations

We are concerned with spectral lines formed by dielectronic capture followed by radiative decay. Including only these two processes and autoionization, the number density, N_l of a state l is given by

$$N_e N_i \varrho_c + \sum_u N_u \Gamma_{ul}^r = N_l (\Gamma_l^a + \Gamma_l^r) \quad (7)$$

where ϱ_c is the rate coefficient for dielectronic capture to state l and Γ_l^a is the autoionization probability of that state, related by

$$\varrho_c = \left(\frac{N_l}{N_e N_i} \right)_S \Gamma_l^a \quad (8)$$

where the subscript S refers to the value of the ratio given by the Saha equation, and N_e and N_i are the number density of electrons and ions respectively. If state l lies below the ionization limit, $\varrho_c = \Gamma_l^a = 0$. Equation 7 can be solved for the populations l by a stepwise downward iteration using the ‘Emissivity’ code [48]. Note that all other processes have been neglected, so that the results obtained here are incomplete for states likely to be populated by radiative recombination or collisional excitation and de-excitation. The results for free-free and free-bound transitions can be used directly to predict line intensities from low-density astrophysical plasmas such as gaseous nebulae but those between bound states underestimate the line intensities in general and should only be used as part of a larger ion population model including all relevant processes.

The emissivity in transition $u \rightarrow l$ is given by

$$\varepsilon_{ul} = N_u \Gamma_{ul}^r h \nu \quad (9)$$

where N_u is the population of the upper state, Γ_{ul}^r is the radiative transition probability between the upper and lower states, h is the Planck’s constant, and ν is the frequency of the transition line. The equivalent effective recombination coefficient ϱ_f , which is linked to the emissivity by the following relation, can also be computed

$$\varrho_f = \frac{\varepsilon}{N_e N_i h \nu} \quad (10)$$

where N_e and N_i are the number density of electrons and ions respectively. In these calculations, all theoretical data for the energy of resonances and bound states were replaced with experimental data from NIST when such experimental data were available.

As part of this investigation, the C II lines from several observational line lists found in the literature, such as that of Zhang *et al* [18] for the planetary nebula NGC 7027, were analyzed using our theoretical line list and all correctly-identified C II recombination lines in these observational lists were identified in our theoretical list apart from very few exceptions which are outside our wavelength range. The analysis also produced an electron temperature for the line-emitting regions of a number of astronomical objects in reasonably good agreement with the values obtained by other researchers using different data and employing other techniques. The details of these investigations will be the subject of a forthcoming paper.

3. Comparison to Previous Work

In this section we make a brief comparison of some of our results against a sample of similar results obtained by other researchers previously. These include radiative transition probabilities, given in Table (C), autoionization probabilities, given in Table (D), and dielectronic recombination coefficients, given in Table (E). Transition probabilities generally show good agreement between the various calculations for the strongest electric dipole transitions. There are some significant differences for intercombination transitions, indicative of the increased uncertainty of the results for these cases. There are also significant differences between the present results and those of Nussbaumer & Storey [6] for some of the allowed but two-electron transitions from the $2s^23p$ configuration, where we would expect our results to be superior, given the larger scattering target.

In Table (D) we compare our calculated autoionization probabilities with those of De Marco *et al* [49]. They combined the LS -coupled autoionization probabilities calculated in the close-coupling approximation by Davey *et al* [16] with one- and two-body fine structure interactions computed with SUPERSTRUCTURE [37] to obtain autoionization probabilities for four states that give rise to spectral lines seen in carbon-rich Wolf-Rayet stars. For the three larger probabilities, there is agreement within 25%. For the $4f\ ^2G_{9/2}^e$ state there is a factor of two difference but this state has a very small autoionization probability corresponding to an energy width of only 4.2×10^{-8} Rydberg.

In Table (E) we compare our results with effective recombination coefficients from Table (1) of Badnell [31]. His results are tabulated between terms, having been summed over the J of the upper and lower terms of the transition, so results for individual lines cannot be compared. Badnell only tabulates results for one transition in which the upper state is allowed to autoionize in LS -coupling ($2s2p(^3P^o)3d\ ^2F^o$) and here the agreement is excellent as one might expect. On the other hand, the two levels of $2s2p(^3P^o)3d\ ^2D^o$ have very small autoionization widths and our coefficients are a factor of $5\times$ smaller than Badnell's for transitions from this term. We note that the fine structure splitting of this term is well represented in our calculation as is its separation from neighboring states with large autoionization widths, giving us confidence in our result.

4. Results

In this section, we present a sample of the data produced during this investigation. In Table (1) the theoretical results for the energies of the bound states of C^+ below the $C^{2+}\ ^1S_0^e$ threshold are given alongside the available experimental data from the NIST database [35]. Similarly, Table (2) presents the energy and autoionization width data for the resonances as obtained by the **K**-matrix and **QB** methods. In these tables, a negative fine structure splitting indicates that the theoretical levels are in reverse order compared to their experimental counterparts. It is noteworthy that due to limited precision of figures in these tables, some data may appear inconsistent, e.g. a zero fine structure splitting from two levels with different energies. Full-precision data in electronic format are available from the Centre de Données astronomiques de Strasbourg (CDS) database.

Regarding the bound states, all levels with effective quantum number between 0.1-13 for the outer electron and $0 \leq l \leq 5$ (142 states) were found. The 8 uppermost bound states in Table (1), i.e. the levels of $2s2p(^3P^o)3d\ ^4F^o$ and $^4D^o$, have quantum numbers higher than 13 and hence are out of range of the **R**-matrix approximation validity; therefore only experimental data are included for these states. Concerning the resonances, we searched for all states with $n < 5$

where n is the principal quantum number of the active electron. 61 levels were found by the **K**-matrix method and 55 by the **QB** method.

Tables (3-5) present a sample of the f -values of the free-bound transitions for some bound symmetries as obtained by integrating photoionization cross section over photon energy where these data are obtained from stage STGBF of the **R**-matrix code. The columns in these tables stand for the bound states identified by their indices as given in Table (1) while the rows stand for the resonances represented by their indices as given in Table (2). An entry of ‘0’ in the f -value tables indicates that no peak was observed in the photoionization cross section data.

Finally, Table (6) contains a sample of the effective recombination coefficients for transitions extracted from our list in a wavelength range where several lines have been observed in the spectra of planetary nebulae [18].

5. Conclusions

In this study, a list of line effective recombination coefficients is generated for the atomic ion C^+ using the **R**-matrix, Autostructure and Emissivity codes. These lines are produced by dielectronic capture and subsequent radiative decays of the low-lying autoionizing states above the threshold of $C^{2+} 1S^e$ with a principal quantum number $n < 5$ for the captured electron. The line list contains 6187 optically-allowed transitions which include many $C II$ lines observed in astronomical spectra, notably the lines of $C II$ in the observational list of Zhang *et al* [18] for the spectrum of planetary nebula NGC 7027. Beside the effective recombination coefficients, the list also include detailed data of level energies for bound and resonance states, and oscillator strengths.

The theoretical results for energy and fine structure splitting agree very well with the available experimental data for both resonances and bound states. The complete data set of our line list can be obtained from the Centre de Données astronomiques de Strasbourg (CDS) database.

In the course of this investigation, a method for finding and analyzing resonances was developed as an alternative to the **QB** [44, 45] and Time-Delay [42] methods. In this one-channel case, the method offers a superior alternative in terms of numerical stability, computational viability and comprehensiveness in the search for the low-lying autoionizing states.

References

- [1] Pottasch S.R.; Wesselius P.R.; van Duinen R.J. Ultraviolet observations of planetary nebulae. IV. The C IV lines at $\lambda 1550 \text{ \AA}$. *Astronomy and Astrophysics*, 70:629–634, 1978.
- [2] Nikitin A.A.; Sapar A.A.; Feklistove T.H.; Kholtygin A.F. Emission-line spectra and the abundance of carbon and nitrogen ions in planetary nebulae. *Soviet Astronomy*, 25(1):56–58, 1981.
- [3] Bogdanovich P.O.; Lukoshiavichius R.A.; Nikitin A.A.; Rudzikas Z.B.; Kholtygin A.F. Lines of carbon, nitrogen, and oxygen ions in the spectra of planetary nebulas. I. Transition probabilities and oscillator strengths. *Astrophysics*, 22(3):326–334, 1985.
- [4] Harrington J.P.; Lutz J.H.; Seaton M.J.; Stickland D.J. Ultraviolet spectra of planetary nebulae - I. The abundance of carbon in IC 418. *Monthly Notices of the Royal Astronomical Society*, 191:13–22, 1980.
- [5] Harrington J.P.; Lutz J.H.; Seaton M.J. Ultraviolet spectra of planetary nebulae. IV - The C III $\lambda 2297$ dielectronic recombination line and dust absorption in the C IV $\lambda 1549$ resonance doublet. *Monthly Notices of the Royal Astronomical Society*, 195:21P–26P, 1981.
- [6] Nussbaumer H.; Storey P.J. C II two-electron transitions. *Astronomy and Astrophysics*, 96(1-2):91–95, 1981.
- [7] Adams S.; Seaton M.J. Ultraviolet spectra of planetary nebulae. VII - The abundance of carbon in the very low excitation nebula He 2-131. *Monthly Notices of the Royal Astronomical Society*, 200:7P–12P, 1982.
- [8] Kholtygin A.F. Carbon Abundance in planetary nebulas. *Astrofizika*, 20(3):503–511, 1984.
- [9] Bogdanovich P.O.; Nikitin A.A.; Rudzikas Z.B.; Kholtygin A.F. Lines of carbon, nitrogen, and oxygen ions in the spectra of planetary nebulas. II - Intensities of the C II and N III recombination lines and abundances of the C III and N IV ions. *Astrofizika*, 23(2):427–435, 1985.
- [10] Boughton W.L. Carbon recombination lines and the neutral hydrogen clouds near the Orion Nebula. *The Astrophysical Journal*, 222:517–526, 1978.
- [11] Peng Y.-L.; Han X.-Y.; Wang M.-S.; Li J.-M. A theoretical study of dielectronic recombination processes of C^{2+} ions in planetary nebulae. *Journal of Physics B*, 38(21):3825–3839, 2005.
- [12] Rola C.; Stasińska G. The carbon abundance problem in planetary nebulae. *Astronomy and Astrophysics*, 282(1):199–212, 1994.
- [13] Clegg R.E.S.; Storey P.J.; Walsh J.R.; Neale L. Measurement of the $^{12}C/^{13}C$ ratio in planetary nebulae. *Monthly Notices of the Royal Astronomical Society*, 284(2):348–358, 1997.
- [14] Nikitin A.A.; Yakubovskii O.A. The Investigation of the N III Recombination Spectrum in Stellar Envelopes and Nebulae. VI. The Equations of Statistical Equilibrium for the Lower Excited Levels of C II, N III, and O IV. *Soviet Astronomy*, 7(2):189–198, 1963.
- [15] Hayes M.A.; Nussbaumer H. The C II infrared and ultraviolet lines. *Astronomy and Astrophysics*, 134(1):193–197, 1984.
- [16] Davey A.R.; Storey P.J.; Kisielius R. Recombination coefficients for C II lines. *Astronomy and Astrophysics*

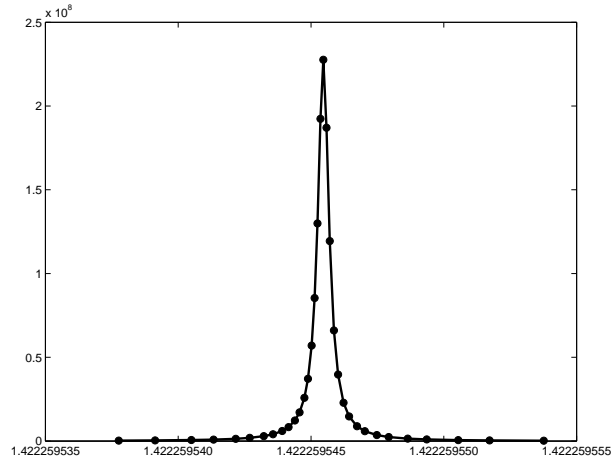
Supplement Series, 142:85–94, 2000.

- [17] Peng Y.-L.; Wang M.-S.; Han X.-Y.; Li J.-M. Theoretic Study of C II Recombination Line. *Chinese Physics Letters*, 21(9):1723–1726, 2004.
- [18] Zhang Y.; Liu X.-W.; Luo S.-G.; Péquignot D.; Barlow M.J. Integrated spectrum of the planetary nebula NGC 7027. *Astronomy and Astrophysics*, 442(1):249–262, 2005.
- [19] Stanghellini L.; Shaw R.A.; Gilmore D. Space Telescope Imaging Spectrograph Ultraviolet Spectra of Large Magellanic Cloud Planetary Nebulae: A Study of Carbon Abundances and Stellar Evolution. *The Astrophysical Journal*, 622(1):294–318, 2005.
- [20] Péquignot D.; Petitjean P.; Boisson C. Total and effective radiative recombination coefficients. *Astronomy and Astrophysics*, 251(2):680–688, 1991.
- [21] Nahar S.N.; Pradhan A.K.; Zhang H.L. Electron-Ion Recombination Rate Coefficients and Photoionization Cross Sections for Astrophysically Abundant Elements. IV. Relativistic Calculations for C IV and C V for Ultraviolet and X-Ray Modeling . *The Astrophysical Journal Supplement Series*, 131(1):375–389, 2000.
- [22] Badnell N.R.; O’Mullane M.G.; Summers H.P.; Altun Z.; Bautista M.A.; Colgan J.; Gorczyca T.W.; Mitnik D.M.; Pindzola M.S.; Zatsarinny O. Dielectronic recombination data for dynamic finite-density plasmas I. Goals and methodology. *Astronomy and Astrophysics*, 406(3):1151–1165, 2003.
- [23] Leibowitz E.M. The emission spectrum of the ion C IV in planetary nebulae. *Monthly Notices of the Royal Astronomical Society*, 157:97–102, 1972.
- [24] Leibowitz E.M. Polarization of C IV emission lines in planetary nebulae. *Monthly Notices of the Royal Astronomical Society*, 157:115–120, 1972.
- [25] Balick B.; Gammon R.H.; Doherty L.H. The Structure of the Orion Nebula. I. Observations of the C 85 α Recombination Line. *The Astrophysical Journal*, 188:45–52, 1974.
- [26] Nussbaumer H.; Storey P.J. The Ionization Balance of C⁰ to C⁺⁴. *Astronomy and astrophysics*, 44:321–327, 1975.
- [27] Clavel J.; Flower D.R.; Seaton M.J. Ultraviolet spectra of planetary nebulae. V - The C II λ 1335 dielectronic recombination lines in IC 418. *Monthly Notices of the Royal Astronomical Society*, 197:301–311, 1981.
- [28] Clegg R.E.S.; Seaton M.J.; Peimbert M.; Torres-Peimbert S. Analysis of nebulosity in the planetary nebula NGC 40. *Monthly Notices of the Royal Astronomical Society*, 205:417–434, 1983.
- [29] Nussbaumer H.; Storey P.J. Dielectronic recombination at low temperatures. II. Recombination coefficients for lines of C, N, O. *Astronomy and Astrophysics Supplement Series*, 56:293–312, 1984.
- [30] Yan Y.; Seaton M.J. Atomic data for opacity calculations. IV. Photoionisation cross sections for C II. *Journal of Physics B*, 20(23):6409–6429, 1987.
- [31] Badnell N.R. The influence of core fine-structure interactions on dielectronic recombination at low temperatures: B-like C, N and O recombined ions. *Journal of Physics B*, 21(5):749–767, 1988.
- [32] Baluteau J.P.; Zavagno A.; Morisset C.; Péquignot D. The 654-1046 NM line spectrum of the planetary nebula

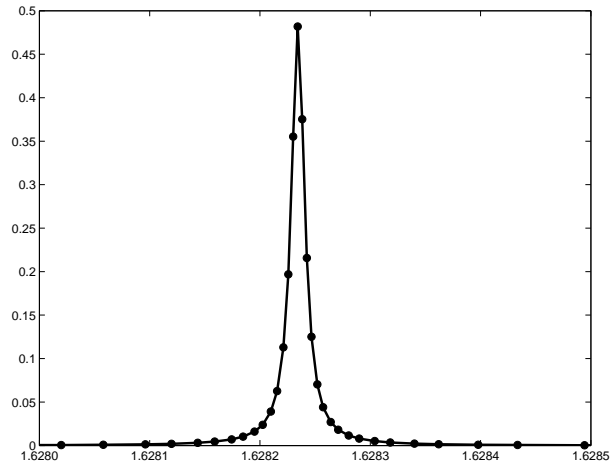
- NGC 7027. *Astronomy and Astrophysics*, 303:175–203, 1995.
- [33] Kholtygin A.F. Inhomogeneous planetary nebulae: carbon and oxygen abundances. *Astronomy and Astrophysics*, 329:691–703, 1998.
- [34] Liu Y.; Liu X.-W.; Barlow M.J.; Luo S.-G. Chemical abundances of planetary nebulae from optical recombination lines - II. Abundances derived from collisionally excited lines and optical recombination lines. *Monthly Notices of the Royal Astronomical Society*, 353(4):1251–1285, 2004.
- [35] National Institute of Standards and Technology (NIST). URL: <http://www.nist.gov>. 2010.
- [36] Berrington K.A.; Eissner W.B.; Norrington P.H. R-MATRIX1: Belfast atomic R-matrix codes. *Computer Physics Communications*, 92(2):290–420, 1995.
- [37] Eissner W.; Jones M.; Nussbaumer H. Techniques for the calculation of atomic structures and radiative data including relativistic corrections. *Computer Physics Communications*, 8(4):270–306, 1974.
- [38] Nussbaumer H.; Storey P.J. The C III transition probabilities. *Astronomy and Astrophysics*, 64(1-2):139–144, 1978.
- [39] Badnell N.R. Autostructure writeup on the world wide web. URL: <http://amdpp.phys.strath.ac.uk/autos/ver/WRITEUP>. 2011.
- [40] Berrington K.A.; Burke P.G.; Dufton P.L.; Kingston A.E. Electron collisional excitation of C III and O V. *Journal of Physics B*, 10(8):1465–1475, 1977.
- [41] Hibbert A. CIV3 - A general program to calculate configuration interaction wave functions and electric-dipole oscillator strengths. *Computer Physics Communications*, 9(3):141–172, 1075.
- [42] Stibbe D.T.; Tennyson J. TIMEDEL: A program for the detection and parameterization of resonances using the time-delay matrix. *Computer Physics Communications*, 114(1-3):236–242, 1998.
- [43] Smith F.T. Lifetime Matrix in Collision Theory. *Physical Review*, 118(1):349–356, 1960.
- [44] Quigley L.; Berrington K. The QB method: analysing resonances using R-matrix theory. Applications to C⁺, He and Li. *Journal of Physics B*, 29(20):4529–4542, 1996.
- [45] Quigley L.; Berrington K.; Pelan J. The QB program: Analysing resonances using R-matrix theory. *Computer Physics Communications*, 114(1-3):225–235, 1998.
- [46] Eissner W.; Nussbaumer H. A programme for calculating atomic structures. *Journal of Physics B*, 2(10):1028–1043, 1969.
- [47] Storey P.J. Dielectronic recombination at nebular temperatures. *Monthly Notices of the Royal Astronomical Society*, 195:27P–31P, 1981.
- [48] Sochi T. Emissivity: A program for atomic transition calculations. *Communications in Computational Physics*, 7(5):1118–1130, 2010.
- [49] De Marco O.; Storey P.J.; Barlow M.J. The WC10 central stars CPD-56 degrees 8032 and He 2-113 - III. Wind electron temperatures and abundances. *Monthly Notices of the Royal Astronomical Society*, 297(4):999–1014, 1997.

- [50] Lennon D.J.; Dufton P.L.; Hibbert A.; Kingston A.E. C II emission lines formed in optically thin plasmas. *The Astrophysical Journal*, 294:200–206, 1985.
- [51] Huber M.C.E.; Sandeman R.J.; Tozzi G.P. Branching Ratios of the $2s^23p\ ^2P^0$ Term of Singly-Ionized Carbon. *Physica Scripta*, T8:95–99, 1984.
- [52] Glenzer S.; Kunze H.-J.; Musielok J.; Kim Y.-K.; Wiese W.L. Investigation of LS coupling in boronlike ions. *Physical Review A*, 49(1):221–227, 1994.
- [53] Fang Z.; Kwong V.H.S.; Wang J. Measurements of radiative-decay rates of the $2s^22p(^2P^o)$ - $2s2p^2(^4P)$ intersystem transitions of C II. *Physical Review A*, 48(2):1114–1122, 1993.
- [54] Dankwort W.; Trefftz E. Breit-Pauli approximation for highly ionized boron-like ions, up to Fe XXII. *Astronomy and Astrophysics*, 65(1):93–98, 1978.

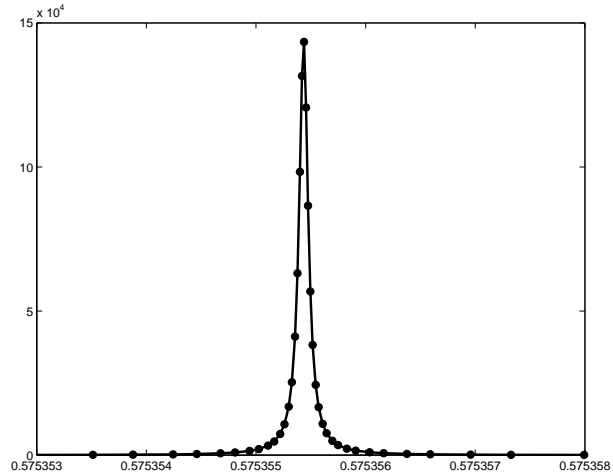
Figures



(a) $2s2p(^3P^o)3d\ ^4P^o_{1/2}$ resonance in $2s2p^2\ ^4P^e_{1/2}$ cross-section.



(b) $2s2p(^3P^o)4d\ ^2F^o_{5/2}$ resonance in $2s2p^2\ ^4P^e_{3/2}$ cross-section.



(c) $2s2p(^3P^o)4p\ ^2P^e_{3/2}$ resonance in $2p^3\ ^2D^o_{5/2}$ cross-section.

Fig. 1: Examples of photoionization cross sections in mega barn (y -axis) of the indicated bound states near to the designated autoionizing states versus photon energy in Rydberg (x -axis).

Table A

The seven orbitals used to construct the C^{2+} target and their STO parameters. The bar marks the pseudo orbitals.

Orbital	C_i	P_i	ξ_i
1s	21.28251	1	5.13180
	6.37632	1	8.51900
	0.08158	2	2.01880
	-2.61339	2	4.73790
	-0.00733	2	1.57130
2s	-5.39193	1	5.13180
	-1.49036	1	8.51900
	5.57151	2	2.01880
	-5.25090	2	4.73790
	0.94247	2	1.57130
$\bar{3}s$	5.69321	1	1.75917
	-19.54864	2	1.75917
	10.39428	3	1.75917
2p	1.01509	2	1.47510
	3.80119	2	3.19410
	2.75006	2	1.83070
	0.89571	2	9.48450
$\bar{3}p$	14.41203	2	1.98138
	-10.88586	3	1.96954
$\bar{3}d$	5.84915	3	2.11997
$\bar{4}f$	9.69136	4	2.69086

Table B

Orbital scaling parameters (λ 's) for Autostructure input. The rows stand for the principal quantum number n , while the columns stand for the orbital angular momentum quantum number l .

	s	p	d	f	g	h
1	1.43240					
2	1.43380	1.39690				
3	1.25760	1.20290	1.35930			
4	1.25830	1.19950	1.35610	1.41460		
5	1.26080	1.20020	1.35770	1.41420	1.32960	
6	1.26370	1.20250	1.36210	1.41520	1.41420	2.34460
7	1.26790					

Table C

A sample of radiative transition probabilities in s^{-1} as obtained from this work compared to corresponding values found in the literature.

Upper	Lower	λ_{vac}	SS	NS	LDHK	HST	GKMKW	FKWP	DT	DSB
$2s2p^2\ 4P^e_{1/2}$	$2s^22p\ 2P^o_{1/2}$	2325.40	52.8	55.3	74.4				42.5	
$2s2p^2\ 4P^e_{3/2}$	$2s^22p\ 2P^o_{1/2}$	2324.21	1.79	1.71	1.70				1.01	
$2s2p^2\ 4P^e_{1/2}$	$2s^22p\ 2P^o_{3/2}$	2328.84	60.6	65.5	77.8				40.2	
$2s2p^2\ 4P^e_{3/2}$	$2s^22p\ 2P^o_{3/2}$	2327.64	9.34	5.24	12.4				8.11	
$2s2p^2\ 4P^e_{5/2}$	$2s^22p\ 2P^o_{3/2}$	2326.11	36.7	43.2	53.9			51.2	34.4	
$2s2p^2\ 2D^e_{3/2}$	$2s^22p\ 2P^o_{1/2}$	1334.53	2.40e8	2.42e8	2.38e8				2.41e8	
$2s2p^2\ 2D^e_{5/2}$	$2s^22p\ 2P^o_{3/2}$	1335.71	2.87e8	2.88e8	2.84e8				2.89e8	
$2s2p^2\ 2D^e_{3/2}$	$2s^22p\ 2P^o_{3/2}$	1335.66	4.75e7	4.78e7	4.70e7				4.79e7	
$2s2p^2\ 2S^e_{1/2}$	$2s^22p\ 2P^o_{1/2}$	1036.34	7.75e8	7.74e8					7.99e8	
$2s2p^2\ 2S^e_{1/2}$	$2s^22p\ 2P^o_{3/2}$	1037.02	1.53e9	1.53e9					1.59e9	
$2s2p^2\ 2P^e_{1/2}$	$2s^22p\ 2P^o_{1/2}$	903.96	2.76e9	2.74e9					2.63e9	
$2s2p^2\ 2P^e_{3/2}$	$2s^22p\ 2P^o_{1/2}$	903.62	6.92e8	6.86e8					6.58e8	
$2s2p^2\ 2P^e_{1/2}$	$2s^22p\ 2P^o_{3/2}$	904.48	1.39e9	1.38e9					1.33e9	
$2s2p^2\ 2P^e_{3/2}$	$2s^22p\ 2P^o_{3/2}$	904.14	3.46e9	3.43e9					3.30e9	
$2s^23s\ 2S^e_{1/2}$	$2s^22p\ 2P^o_{1/2}$	858.09	1.26e8	1.31e8					3.69e7	
$2s^23s\ 2S^e_{1/2}$	$2s^22p\ 2P^o_{3/2}$	858.56	2.46e8	2.58e8					1.11e8	
$2s^23p\ 2P^o_{1/2}$	$2s2p^2\ 4P^e_{1/2}$	1127.13	36.3	55.5						
$2s^23p\ 2P^o_{3/2}$	$2s2p^2\ 4P^e_{1/2}$	1126.99	58.28	97.8						
$2s^23p\ 2P^o_{1/2}$	$2s2p^2\ 4P^e_{3/2}$	1127.41	21.8	20.3						
$2s^23p\ 2P^o_{3/2}$	$2s2p^2\ 4P^e_{3/2}$	1127.27	14.0	22.3						
$2s^23p\ 2P^o_{3/2}$	$2s2p^2\ 4P^e_{5/2}$	1127.63	1.86e2	2.60e2						
$2p^3\ 4S^o_{3/2}$	$2s2p^2\ 4P^e_{1/2}$	1009.86	5.77e8	5.82e8					5.76e8	
$2p^3\ 4S^o_{3/2}$	$2s2p^2\ 4P^e_{3/2}$	1010.08	1.15e9	1.16e9					1.15e9	
$2p^3\ 4S^o_{3/2}$	$2s2p^2\ 4P^e_{5/2}$	1010.37	1.73e9	1.74e9					1.73e9	
$2s^23p\ 2P^o_{3/2}$	$2s2p^2\ 2D^e_{5/2}$	1760.40	3.77e7	3.75e7		4.3e7				
$2s^23p\ 2P^o_{1/2}$	$2s2p^2\ 2D^e_{3/2}$	1760.82	4.19e7	4.16e7		5.2e7				
$2s^23p\ 2P^o_{3/2}$	$2s2p^2\ 2D^e_{3/2}$	1760.47	4.18e6	4.16e6		4e6				
$2p^3\ 4S^o_{3/2}$	$2s2p^2\ 2D^e_{5/2}$	1490.38	1.03e2	45.0						
$2p^3\ 4S^o_{3/2}$	$2s2p^2\ 2D^e_{3/2}$	1490.44	10.5	11.9						
$2s^23p\ 2P^o_{1/2}$	$2s2p^2\ 2S^e_{1/2}$	2838.44	3.61e7	3.63e7		2.2e7				
$2s^23p\ 2P^o_{3/2}$	$2s2p^2\ 2S^e_{1/2}$	2837.54	3.61e7	3.64e7		2.2e7				
$2p^3\ 4S^o_{3/2}$	$2s2p^2\ 2S^e_{1/2}$	2196.19	1.62	5.09						
$2s^23p\ 2P^o_{1/2}$	$2s2p^2\ 2P^e_{1/2}$	4739.29	5.85e4	7.70e4		<3.0e5				
$2s^23p\ 2P^o_{3/2}$	$2s2p^2\ 2P^e_{1/2}$	4736.79	7.98e3	1.19e4		<5e5				
$2s^23p\ 2P^o_{1/2}$	$2s2p^2\ 2P^e_{3/2}$	4748.61	2.35e4	3.23e4		<2.3e5				
$2s^23p\ 2P^o_{3/2}$	$2s2p^2\ 2P^e_{3/2}$	4746.09	6.08e4	8.28e4		<1.3e5				
$2p^3\ 4S^o_{3/2}$	$2s2p^2\ 2P^e_{1/2}$	3184.42	16.4	14.9						
$2p^3\ 4S^o_{3/2}$	$2s2p^2\ 2P^e_{3/2}$	3188.62	80.0	76.9						
$2s^23p\ 2P^o_{1/2}$	$2s^23s\ 2S^e_{1/2}$	6584.70	3.53e7	3.68e7		2.9e7	3.29e7			
$2s^23p\ 2P^o_{3/2}$	$2s^23s\ 2S^e_{1/2}$	6579.87	3.54e7	3.69e7		3.4e7	3.33e7			
$2p^3\ 4S^o_{3/2}$	$2s^23s\ 2S^e_{1/2}$	3923.19	6.35	10.2						
$2s^23d\ 2D^e_{3/2}$	$2s^23p\ 2P^o_{1/2}$	7233.33	3.46e7				4.22e7			
$2s^23d\ 2D^e_{3/2}$	$2s^23p\ 2P^o_{3/2}$	7239.16	6.91e6				8.49e6			
$2s^23d\ 2D^e_{5/2}$	$2s^23p\ 2P^o_{3/2}$	7238.41	4.15e7				5.10e7			
$2s^23d\ 2D^e_{3/2}$	$2s^22p\ 2P^o_{1/2}$	687.05	2.40e9						2.24e9	
$2s^23d\ 2D^e_{3/2}$	$2s^22p\ 2P^o_{3/2}$	687.35	4.81e8						4.50e8	
$2s^23d\ 2D^e_{5/2}$	$2s^22p\ 2P^o_{3/2}$	687.35	2.88e9						2.70e9	
$2p^3\ 2D^o_{3/2}$	$2s2p^2\ 2D^e_{3/2}$	1323.91	4.33e8						4.53e8	
$2p^3\ 2D^o_{5/2}$	$2s2p^2\ 2D^e_{3/2}$	1324.00	3.23e7						3.38e7	
$2p^3\ 2D^o_{3/2}$	$2s2p^2\ 2D^e_{5/2}$	1323.86	4.91e7						5.10e7	
$2p^3\ 2D^o_{5/2}$	$2s2p^2\ 2D^e_{5/2}$	1323.95	4.51e8						4.71e8	
$2p^3\ 2D^o_{3/2}$	$2s2p^2\ 2P^e_{1/2}$	2509.88	4.53e7						5.38e7	
$2p^3\ 2D^o_{3/2}$	$2s2p^2\ 2P^e_{3/2}$	2512.49	8.91e6						1.06e7	
$2p^3\ 2D^o_{5/2}$	$2s2p^2\ 2P^e_{3/2}$	2512.81	5.40e7						6.43e7	
$2s2p(3P^o)4f\ 2D^e_{5/2}$	$2s2p(3P^o)3d\ 2P^o_{3/2}$	5115.07	1.18e8							6.94e7
$2s2p(3P^o)4f\ 2G^e_{9/2}$	$2s2p(3P^o)3d\ 2F^o_{7/2}$	4620.54	2.29e8							1.84e8
$2s2p(3P^o)3d\ 2P^o_{3/2}$	$2s2p(3P^o)3p\ 2P^e_{3/2}$	4966.12	3.14e7	18					2.89e7	
$2s2p(3P^o)3d\ 2F^o_{7/2}$	$2s2p(3P^o)3p\ 2D^e_{5/2}$	8796.49	2.03e7						1.99e7	

SS = current work, NS = Nussbaumer and Storey [6]; LDHK = Lennon *et al* [50]; HST = Huber *et al* [51]; GKMKW = Glenzer *et al* [52]; FKWP = Fang *et al* [53]; DT =

Dankwort and Treffitz [54], DSB = De Marco *et al* [49].

Table D

Autoionization probabilities in s^{-1} of four resonance states as obtained in the current work (SS) compared to those obtained by De Marco *et al* [49] (DSB).

State	SS	DSB
$2s2p(^3P^o)4f\ ^2D_{5/2}^e$	9.860e10	8.263e10
$2s2p(^3P^o)4f\ ^2G_{9/2}^e$	8.601e8	1.623e9
$2s2p(^3P^o)3d\ ^2P_{3/2}^o$	2.194e11	1.901e11
$2s2p(^3P^o)3d\ ^2F_{7/2}^o$	1.196e12	1.488e12

Table E

Effective dielectronic recombination rate coefficients in $\text{cm}^3 \cdot \text{s}^{-1}$ of a number of transitions for the given logarithmic temperatures. The first row for each transition corresponds to Badnell [31], while the second row is obtained from the current work. The superscripts denote powers of 10.

		$\log_{10}(T)$									
Upper	Lower	3.0	3.2	3.4	3.6	3.8	4.0	4.2	4.4	4.6	4.8
2s2p(³ P ^o)3d ⁴ F ^o	2s2p(³ P ^o)3p ⁴ D ^e	7.27 ⁻²⁴	5.73 ⁻²⁰	1.56 ⁻¹⁷	6.17 ⁻¹⁶	6.47 ⁻¹⁵	2.61 ⁻¹⁴	5.52 ⁻¹⁴	7.43 ⁻¹⁴	7.25 ⁻¹⁴	5.65 ⁻¹⁴
		6.74 ⁻²⁴	5.17 ⁻²⁰	1.29 ⁻¹⁷	4.33 ⁻¹⁶	3.90 ⁻¹⁵	1.33 ⁻¹⁴	2.31 ⁻¹⁴	2.57 ⁻¹⁴	2.13 ⁻¹⁴	1.47 ⁻¹⁴
2s2p(³ P ^o)3p ⁴ D ^e	2s2p(³ P ^o)3s ⁴ P ^o	1.90 ⁻¹⁶	3.21 ⁻¹⁶	8.53 ⁻¹⁶	4.95 ⁻¹⁵	1.93 ⁻¹⁴	4.90 ⁻¹⁴	8.51 ⁻¹⁴	1.05 ⁻¹³	9.91 ⁻¹⁴	7.57 ⁻¹⁴
		1.06 ⁻¹⁶	1.90 ⁻¹⁶	7.71 ⁻¹⁶	5.02 ⁻¹⁵	1.74 ⁻¹⁴	3.58 ⁻¹⁴	4.85 ⁻¹⁴	4.76 ⁻¹⁴	3.70 ⁻¹⁴	2.46 ⁻¹⁴
2s2p(³ P ^o)3d ² D ^o	2s2p(³ P ^o)3p ² P ^e	2.49 ⁻¹⁴	3.19 ⁻¹⁴	2.90 ⁻¹⁴	2.11 ⁻¹⁴	1.35 ⁻¹⁴	8.05 ⁻¹⁵	4.80 ⁻¹⁵	2.94 ⁻¹⁵	1.81 ⁻¹⁵	1.10 ⁻¹⁵
		4.67 ⁻¹⁵	5.99 ⁻¹⁵	5.44 ⁻¹⁵	3.97 ⁻¹⁵	2.58 ⁻¹⁵	1.68 ⁻¹⁵	1.17 ⁻¹⁵	8.31 ⁻¹⁶	5.54 ⁻¹⁶	3.41 ⁻¹⁶
2s2p(³ P ^o)3p ⁴ P ^e	2s2p(³ P ^o)3s ⁴ P ^o	3.08 ⁻¹⁶	5.09 ⁻¹⁶	9.86 ⁻¹⁶	4.02 ⁻¹⁵	1.08 ⁻¹⁴	1.73 ⁻¹⁴	2.04 ⁻¹⁴	1.97 ⁻¹⁴	1.61 ⁻¹⁴	1.14 ⁻¹⁴
		1.49 ⁻¹⁶	2.52 ⁻¹⁶	7.24 ⁻¹⁶	3.84 ⁻¹⁵	1.05 ⁻¹⁴	1.58 ⁻¹⁴	1.60 ⁻¹⁴	1.27 ⁻¹⁴	8.52 ⁻¹⁵	5.14 ⁻¹⁵
2s2p(³ P ^o)4f ² F ^e	2s2p(³ P ^o)3d ² D ^o	3.00 ⁻²⁷	6.39 ⁻²²	1.14 ⁻¹⁸	9.93 ⁻¹⁷	1.29 ⁻¹⁵	5.09 ⁻¹⁵	9.43 ⁻¹⁵	1.09 ⁻¹⁴	9.26 ⁻¹⁵	6.51 ⁻¹⁵
		1.64 ⁻²⁷	3.53 ⁻²²	6.33 ⁻¹⁹	5.54 ⁻¹⁷	7.22 ⁻¹⁶	2.82 ⁻¹⁵	5.18 ⁻¹⁵	5.88 ⁻¹⁵	4.94 ⁻¹⁵	3.43 ⁻¹⁵
2s2p(³ P ^o)4f ⁴ D ^e	2s2p(³ P ^o)3d ⁴ P ^o	2.56 ⁻²⁷	7.68 ⁻²²	1.70 ⁻¹⁸	1.70 ⁻¹⁶	2.40 ⁻¹⁵	9.95 ⁻¹⁵	1.90 ⁻¹⁴	2.21 ⁻¹⁴	1.89 ⁻¹⁴	1.33 ⁻¹⁴
		2.54 ⁻²⁷	7.63 ⁻²²	1.69 ⁻¹⁸	1.69 ⁻¹⁶	2.39 ⁻¹⁵	9.86 ⁻¹⁵	1.87 ⁻¹⁴	2.17 ⁻¹⁴	1.85 ⁻¹⁴	1.29 ⁻¹⁴
2s2p(³ P ^o)4s ⁴ P ^o	2s2p(³ P ^o)3p ⁴ P ^e	2.59 ⁻²⁰	1.23 ⁻¹⁷	4.65 ⁻¹⁶	3.58 ⁻¹⁵	1.01 ⁻¹⁴	1.51 ⁻¹⁴	1.51 ⁻¹⁴	1.18 ⁻¹⁴	7.80 ⁻¹⁵	4.67 ⁻¹⁵
		2.63 ⁻²⁰	1.25 ⁻¹⁷	4.72 ⁻¹⁶	3.63 ⁻¹⁵	1.02 ⁻¹⁴	1.53 ⁻¹⁴	1.53 ⁻¹⁴	1.19 ⁻¹⁴	7.83 ⁻¹⁵	4.68 ⁻¹⁵
2s2p(³ P ^o)4f ⁴ F ^e	2s2p(³ P ^o)3d ⁴ D ^o	5.39 ⁻²⁷	1.16 ⁻²¹	2.07 ⁻¹⁸	1.81 ⁻¹⁶	2.37 ⁻¹⁵	9.41 ⁻¹⁵	1.77 ⁻¹⁴	2.07 ⁻¹⁴	1.79 ⁻¹⁴	1.27 ⁻¹⁴
		3.48 ⁻²⁷	7.51 ⁻²²	1.35 ⁻¹⁸	1.19 ⁻¹⁶	1.55 ⁻¹⁵	6.07 ⁻¹⁵	1.11 ⁻¹⁴	1.26 ⁻¹⁴	1.06 ⁻¹⁴	7.37 ⁻¹⁵
2s2p(³ P ^o)4f ⁴ G ^e	2s2p(³ P ^o)3d ⁴ F ^o	5.42 ⁻²⁷	1.50 ⁻²¹	3.15 ⁻¹⁸	3.05 ⁻¹⁶	4.24 ⁻¹⁵	1.74 ⁻¹⁴	3.30 ⁻¹⁴	3.86 ⁻¹⁴	3.32 ⁻¹⁴	2.34 ⁻¹⁴
		2.98 ⁻²⁷	8.25 ⁻²²	1.73 ⁻¹⁸	1.68 ⁻¹⁶	2.33 ⁻¹⁵	9.49 ⁻¹⁵	1.78 ⁻¹⁴	2.06 ⁻¹⁴	1.75 ⁻¹⁴	1.22 ⁻¹⁴
2s2p(³ P ^o)4s ⁴ P ^o	2s2p(³ P ^o)3p ⁴ D ^e	2.86 ⁻²⁰	1.36 ⁻¹⁷	5.14 ⁻¹⁶	3.95 ⁻¹⁵	1.11 ⁻¹⁴	1.67 ⁻¹⁴	1.67 ⁻¹⁴	1.30 ⁻¹⁴	8.61 ⁻¹⁵	5.15 ⁻¹⁵
		3.15 ⁻²⁰	1.49 ⁻¹⁷	5.65 ⁻¹⁶	4.35 ⁻¹⁵	1.22 ⁻¹⁴	1.83 ⁻¹⁴	1.83 ⁻¹⁴	1.42 ⁻¹⁴	9.37 ⁻¹⁵	5.59 ⁻¹⁵
2s2p(³ P ^o)4d ⁴ F ^o	2s2p(³ P ^o)3p ⁴ D ^e	1.77 ⁻²⁶	1.71 ⁻²¹	1.85 ⁻¹⁸	1.18 ⁻¹⁶	1.30 ⁻¹⁵	4.85 ⁻¹⁵	9.35 ⁻¹⁵	1.18 ⁻¹⁴	1.10 ⁻¹⁴	8.31 ⁻¹⁵
		1.75 ⁻²⁶	1.69 ⁻²¹	1.83 ⁻¹⁸	1.17 ⁻¹⁶	1.24 ⁻¹⁵	4.28 ⁻¹⁵	7.25 ⁻¹⁵	7.83 ⁻¹⁵	6.37 ⁻¹⁵	4.34 ⁻¹⁵
2s2p ² ² D ^e	2s ² 2p ² P ^o	2.45 ⁻¹²	5.89 ⁻¹²	8.34 ⁻¹²	8.17 ⁻¹²	6.33 ⁻¹²	4.36 ⁻¹²	3.01 ⁻¹²	2.21 ⁻¹²	1.66 ⁻¹²	1.19 ⁻¹²
		1.85 ⁻¹²	5.12 ⁻¹²	7.66 ⁻¹²	7.67 ⁻¹²	6.00 ⁻¹²	4.09 ⁻¹²	2.61 ⁻¹²	1.60 ⁻¹²	9.38 ⁻¹³	5.28 ⁻¹³
2s2p(³ P ^o)3d ² D ^o	2s2p ² ² P ^e	2.60 ⁻¹³	3.33 ⁻¹³	3.02 ⁻¹³	2.20 ⁻¹³	1.41 ⁻¹³	8.41 ⁻¹⁴	5.01 ⁻¹⁴	3.07 ⁻¹⁴	1.89 ⁻¹⁴	1.15 ⁻¹⁴
		4.50 ⁻¹⁴	5.78 ⁻¹⁴	5.24 ⁻¹⁴	3.83 ⁻¹⁴	2.49 ⁻¹⁴	1.62 ⁻¹⁴	1.13 ⁻¹⁴	8.01 ⁻¹⁵	5.34 ⁻¹⁵	3.29 ⁻¹⁵
2s2p(³ P ^o)4d ² D ^o	2s2p ² ² P ^e	6.56 ⁻²⁷	1.10 ⁻²¹	1.70 ⁻¹⁸	1.35 ⁻¹⁶	1.66 ⁻¹⁵	6.33 ⁻¹⁵	1.16 ⁻¹⁴	1.33 ⁻¹⁴	1.13 ⁻¹⁴	8.02 ⁻¹⁵
		1.98 ⁻²⁷	3.29 ⁻²²	5.03 ⁻¹⁹	3.97 ⁻¹⁷	4.85 ⁻¹⁶	1.82 ⁻¹⁵	3.26 ⁻¹⁵	3.64 ⁻¹⁵	3.03 ⁻¹⁵	2.09 ⁻¹⁵
2s2p ² ² P ^e	2s ² 2p ² P ^o	2.68 ⁻¹³	3.99 ⁻¹³	5.05 ⁻¹³	5.45 ⁻¹³	4.87 ⁻¹³	3.95 ⁻¹³	3.37 ⁻¹³	3.09 ⁻¹³	2.75 ⁻¹³	2.21 ⁻¹³
		5.11 ⁻¹⁴	1.11 ⁻¹³	2.21 ⁻¹³	3.09 ⁻¹³	3.18 ⁻¹³	2.78 ⁻¹³	2.24 ⁻¹³	1.66 ⁻¹³	1.11 ⁻¹³	6.82 ⁻¹⁴
2s2p(³ P ^o)3d ² D ^o	2s2p ² ² D ^e	7.38 ⁻¹³	9.47 ⁻¹³	8.59 ⁻¹³	6.26 ⁻¹³	3.99 ⁻¹³	2.39 ⁻¹³	1.42 ⁻¹³	8.71 ⁻¹⁴	5.38 ⁻¹⁴	3.25 ⁻¹⁴
		1.36 ⁻¹³	1.75 ⁻¹³	1.59 ⁻¹³	1.16 ⁻¹³	7.53 ⁻¹⁴	4.90 ⁻¹⁴	3.43 ⁻¹⁴	2.42 ⁻¹⁴	1.61 ⁻¹⁴	9.95 ⁻¹⁵
2s2p(³ P ^o)3s ⁴ P ^o	2s2p ² ⁴ P ^e	1.36 ⁻¹⁵	2.22 ⁻¹⁵	3.36 ⁻¹⁵	1.07 ⁻¹⁴	3.30 ⁻¹⁴	7.13 ⁻¹⁴	1.12 ⁻¹³	1.32 ⁻¹³	1.21 ⁻¹³	9.09 ⁻¹⁴
		7.17 ⁻¹⁶	1.19 ⁻¹⁵	2.35 ⁻¹⁵	1.02 ⁻¹⁴	3.12 ⁻¹⁴	5.78 ⁻¹⁴	7.22 ⁻¹⁴	6.71 ⁻¹⁴	5.05 ⁻¹⁴	3.29 ⁻¹⁴
2s2p(³ P ^o)3d ² F ^o	2s2p ² ² D ^e	1.70 ⁻¹²	4.92 ⁻¹²	7.44 ⁻¹²	7.49 ⁻¹²	5.83 ⁻¹²	3.86 ⁻¹²	2.30 ⁻¹²	1.29 ⁻¹²	6.93 ⁻¹³	3.63 ⁻¹³
		1.71 ⁻¹²	4.94 ⁻¹²	7.48 ⁻¹²	7.53 ⁻¹²	5.86 ⁻¹²	3.88 ⁻¹²	2.32 ⁻¹²	1.30 ⁻¹²	6.97 ⁻¹³	3.65 ⁻¹³
2s2p(³ P ^o)4d ² D ^o	2s2p ² ² D ^e	2.30 ⁻²⁶	3.86 ⁻²¹	5.94 ⁻¹⁸	4.72 ⁻¹⁶	5.81 ⁻¹⁵	2.22 ⁻¹⁴	4.05 ⁻¹⁴	4.65 ⁻¹⁴	3.97 ⁻¹⁴	2.81 ⁻¹⁴
		9.59 ⁻²⁷	1.59 ⁻²¹	2.43 ⁻¹⁸	1.92 ⁻¹⁶	2.35 ⁻¹⁵	8.82 ⁻¹⁵	1.58 ⁻¹⁴	1.76 ⁻¹⁴	1.47 ⁻¹⁴	1.01 ⁻¹⁴
2s2p(³ P ^o)3d ⁴ D ^o	2s2p ² ⁴ P ^e	2.49 ⁻²⁴	2.83 ⁻²⁰	1.05 ⁻¹⁷	4.56 ⁻¹⁶	4.63 ⁻¹⁵	1.78 ⁻¹⁴	3.62 ⁻¹⁴	4.76 ⁻¹⁴	4.58 ⁻¹⁴	3.53 ⁻¹⁴
		2.34 ⁻²⁴	2.63 ⁻²⁰	9.38 ⁻¹⁸	3.84 ⁻¹⁶	3.62 ⁻¹⁵	1.23 ⁻¹⁴	2.11 ⁻¹⁴	2.32 ⁻¹⁴	1.91 ⁻¹⁴	1.31 ⁻¹⁴
2s2p(³ P ^o)3d ⁴ P ^o	2s2p ² ⁴ P ^e	6.71 ⁻¹⁴	1.08 ⁻¹³	1.13 ⁻¹³	9.07 ⁻¹⁴	6.36 ⁻¹⁴	4.86 ⁻¹⁴	4.61 ⁻¹⁴	4.51 ⁻¹⁴	3.87 ⁻¹⁴	2.84 ⁻¹⁴
		3.41 ⁻¹⁴	5.51 ⁻¹⁴	5.78 ⁻¹⁴	4.63 ⁻¹⁴	3.38 ⁻¹⁴	2.97 ⁻¹⁴	3.10 ⁻¹⁴	2.93 ⁻¹⁴	2.30 ⁻¹⁴	1.55 ⁻¹⁴
2s2p(³ P ^o)4s ⁴ P ^o	2s2p ² ⁴ P ^e	9.12 ⁻²⁰	4.32 ⁻¹⁷	1.64 ⁻¹⁵	1.26 ⁻¹⁴	3.55 ⁻¹⁴	5.31 ⁻¹⁴	5.33 ⁻¹⁴	4.14 ⁻¹⁴	2.75 ⁻¹⁴	1.64 ⁻¹⁴
		1.13 ⁻¹⁹	5.37 ⁻¹⁷	2.03 ⁻¹⁵	1.56 ⁻¹⁴	4.40 ⁻¹⁴	6.58 ⁻¹⁴	6.59 ⁻¹⁴	5.12 ⁻¹⁴	3.38 ⁻¹⁴	2.02 ⁻¹⁴
2s2p(³ P ^o)4d ⁴ D ^o	2s2p ² ⁴ P ^e	4.87 ⁻²⁶	6.33 ⁻²¹	8.27 ⁻¹⁸	5.94 ⁻¹⁶	6.90 ⁻¹⁵	2.57 ⁻¹⁴	4.72 ⁻¹⁴	5.54 ⁻¹⁴	4.85 ⁻¹⁴	3.49 ⁻¹⁴
		1.73 ⁻²⁶	2.26 ⁻²¹	2.95 ⁻¹⁸	2.12 ⁻¹⁶	2.43 ⁻¹⁵	8.79 ⁻¹⁵	1.53 ⁻¹⁴	1.69 ⁻¹⁴	1.39 ⁻¹⁴	9.52 ⁻¹⁵
2s2p(³ P ^o)4d ⁴ P ^o	2s2p ² ⁴ P ^e	5.09 ⁻²⁷	9.49 ⁻²²	1.56 ⁻¹⁸	1.30 ⁻¹⁶	1.68 ⁻¹⁵	6.90 ⁻¹⁵	1.39 ⁻¹⁴	1.78 ⁻¹⁴	1.67 ⁻¹⁴	1.27 ⁻¹⁴
		4.37 ⁻²⁸	8.18 ⁻²³	1.34 ⁻¹⁹	1.11 ⁻¹⁷	1.40 ⁻¹⁶	5.37 ⁻¹⁶	9.70 ⁻¹⁶	1.09 ⁻¹⁵	9.13 ⁻¹⁶	6.32 ⁻¹⁶
2s2p(³ P ^o)3p ² P ^e	2s ² 2p ² P ^o	1.91 ⁻¹⁴	2.70 ⁻¹⁴	3.11 ⁻¹⁴	3.17 ⁻¹⁴	2.97 ⁻¹⁴	2.65 ⁻¹⁴	2.26 ⁻¹⁴	1.81 ⁻¹⁴	1.34 ⁻¹⁴	9.18 ⁻¹⁵
		4.59 ⁻¹⁵	9.59 ⁻¹⁵	1.86 ⁻¹⁴	2.67 ⁻¹⁴	2.99 ⁻¹⁴	2.83 ⁻¹⁴	2.31 ⁻¹⁴	1.66 ⁻¹⁴	1.06 ⁻¹⁴	6.26 ⁻¹⁵
2s2p(³ P ^o)4p ² P ^e	2s ² 2p ² P ^o	5.81 ⁻²³	3.67 ⁻¹⁹	7.12 ⁻¹⁷	1.53 ⁻¹⁵	8.24 ⁻¹⁵	1.85 ⁻¹⁴	2.40 ⁻¹⁴	2.19 ⁻¹⁴	1.61 ⁻¹⁴	1.03 ⁻¹⁴
		6.35 ⁻²³	3.96 ⁻¹⁹	7.62 ⁻¹⁷	1.63 ⁻¹⁵	8.74 ⁻¹⁵	1.96 ⁻¹⁴	2.52 ⁻¹⁴	2.30 ⁻¹⁴	1.68 ⁻¹⁴	1.07 ⁻¹⁴

Table 1

The available experimental data from NIST for the bound states of C^+ below the $C^{2+} 1S_0^e$ threshold alongside the theoretical results from **R-matrix** calculations.

In. ^a	Config. ^b	Level	NEEW ^c	NEER ^d	FSS ^e	TER ^f	FSSR ^g
1	2s ² 2p	$2P_{1/2}^o$	0	-1.792141		-1.792571	
2	2s ² 2p	$2P_{3/2}^o$	63.42	-1.791563	63.4	-1.791994	63.3
3	2s2p ²	$4P_{1/2}^e$	43003.3	-1.400266		-1.401292	
4	2s2p ²	$4P_{3/2}^e$	43025.3	-1.400065		-1.401090	
5	2s2p ²	$4P_{5/2}^e$	43053.6	-1.399807	50.3	-1.400755	59.0
6	2s2p ²	$2D_{5/2}^e$	74930.1	-1.109327		-1.105247	
7	2s2p ²	$2D_{3/2}^e$	74932.62	-1.109304	2.5	-1.105266	-2.1
8	2s2p ²	$2S_{1/2}^e$	96493.74	-0.912825		-0.899439	
9	2s2p ²	$2P_{1/2}^e$	110624.17	-0.784059		-0.772978	
10	2s2p ²	$2P_{3/2}^e$	110665.56	-0.783682	41.4	-0.772570	44.8
11	2s ² 3s	$2S_{1/2}^e$	116537.65	-0.730171		-0.727698	
12	2s ² 3p	$2P_{1/2}^o$	131724.37	-0.591780		-0.592081	
13	2s ² 3p	$2P_{3/2}^o$	131735.52	-0.591678	11.1	-0.591980	11.1
14	2p ³	$4S_{3/2}^o$	142027.1	-0.497894		-0.487491	
15	2s ² 3d	$2D_{3/2}^e$	145549.27	-0.465798		-0.466024	
16	2s ² 3d	$2D_{5/2}^e$	145550.7	-0.465785	1.4	-0.466005	2.1
17	2p ³	$2D_{5/2}^o$	150461.58	-0.421034		-0.412359	
18	2p ³	$2D_{3/2}^o$	150466.69	-0.420987	5.1	-0.412388	-3.1
19	2s ² 4s	$2S_{1/2}^e$	157234.07	-0.359318		-0.358955	
20	2s ² 4p	$2P_{1/2}^o$	162517.89	-0.311169		-0.310784	
21	2s ² 4p	$2P_{3/2}^o$	162524.57	-0.311108	6.7	-0.310723	6.6
22	2s2p(³ P ^o)3s	$4P_{1/2}^o$	166967.13	-0.270624		-0.268893	
23	2s2p(³ P ^o)3s	$4P_{3/2}^o$	166990.73	-0.270409		-0.268645	
24	2s2p(³ P ^o)3s	$4P_{5/2}^o$	167035.71	-0.269999	68.6	-0.268229	72.9
25	2s ² 4d	$2D_{3/2}^e$	168123.74	-0.260084		-0.260084	
26	2s ² 4d	$2D_{5/2}^e$	168124.45	-0.260078	0.7	-0.260074	1.1
27	2p ³	$2P_{1/2}^o$	168729.53	-0.254564		-0.245329	
28	2p ³	$2P_{3/2}^o$	168748.3	-0.254393	18.8	-0.245083	27.1
29	2s ² 4f	$2F_{5/2}^o$	168978.34	-0.252297		-0.252162	
30	2s ² 4f	$2F_{7/2}^o$	168978.34	-0.252297	0.0	-0.252160	0.2
31	2s ² 5s	$2S_{1/2}^e$	173347.84	-0.212479		-0.212278	
32	2s ² 5p	$2P_{1/2}^o$	175287.39	-0.194804		-0.190099	
33	2s ² 5p	$2P_{3/2}^o$	175294.75	-0.194737	7.4	-0.190072	3.0
34	2s2p(³ P ^o)3s	$2P_{1/2}^o$	177774.59	-0.172139		-0.165330	
35	2s2p(³ P ^o)3s	$2P_{3/2}^o$	177793.54	-0.171967	19.0	-0.165143	20.5
36	2s ² 5d	$2D_{3/2}^e$	178495.11	-0.165573		-0.165606	
37	2s ² 5d	$2D_{5/2}^e$	178495.71	-0.165568	0.6	-0.165599	0.8
38	2s ² 5f	$2F_{5/2}^o$	178955.94	-0.161374		-0.161296	
39	2s ² 5f	$2F_{7/2}^o$	178955.94	-0.161374	0.0	-0.161295	0.1
40	2s ² 5g	$2G_{7/2}^e$	179073.05	-0.160307		-0.160184	
41	2s ² 5g	$2G_{9/2}^e$	179073.05	-0.160307	0.0	-0.160184	0.0
42	2s ² 6s	$2S_{1/2}^e$	181264.24	-0.140339		-0.140231	

Table 1 continued.

In.	Config.	Level	NEEW	NEER	FSS	TER	FSSR
43	2s2p(³ P ^o)3p	⁴ D ^e _{1/2}	181696.66	-0.136399		-0.136848	
44	2s2p(³ P ^o)3p	⁴ D ^e _{3/2}	181711.03	-0.136268		-0.136699	
45	2s2p(³ P ^o)3p	⁴ D ^e _{5/2}	181736.05	-0.136040		-0.136454	
46	2s2p(³ P ^o)3p	⁴ D ^e _{7/2}	181772.41	-0.135709	75.8	-0.136115	80.4
47	2s2p(³ P ^o)3p	² P ^e _{1/2}	182023.86	-0.133417		-0.133095	
48	2s2p(³ P ^o)3p	² P ^e _{3/2}	182043.41	-0.133239	19.6	-0.132896	21.8
49	2s ² 6p	² P ^o _{1/2}	182993.23	-0.124584		-0.124376	
50	2s ² 6p	² P ^o _{3/2}	182993.66	-0.124580	0.4	-0.124351	2.7
51	2s ² 6d	² D ^e _{3/2}	184074.59	-0.114730		-0.114739	
52	2s ² 6d	² D ^e _{5/2}	184075.28	-0.114723	0.7	-0.114729	1.0
53	2s ² 6f	² F ^o _{5/2}	184376.06	-0.111982		-0.111924	
54	2s ² 6f	² F ^o _{7/2}	184376.06	-0.111982	0.0	-0.111924	0.1
55	2s ² 6g	² G ^e _{7/2}	184449.27	-0.111315		-0.111264	
56	2s ² 6g	² G ^e _{9/2}	184449.27	-0.111315	0.0	-0.111264	0.0
57	2s ² 6h	² H ^o _{9/2}	184466.5	-0.111158		-0.111122	
58	2s ² 6h	² H ^o _{11/2}	184466.5	-0.111158	0.0	-0.111122	0.0
59	2s2p(³ P ^o)3p	⁴ S ^e _{3/2}	184690.98	-0.109113		-0.108410	
60	2s ² 7s	² S ^e _{1/2}	185732.93	-0.099618		-0.099537	
61	2s2p(³ P ^o)3p	⁴ P ^e _{1/2}	186427.35	-0.093290		-0.092097	
62	2s2p(³ P ^o)3p	⁴ P ^e _{3/2}	186443.69	-0.093141		-0.091950	
63	2s2p(³ P ^o)3p	⁴ P ^e _{5/2}	186466.02	-0.092937	38.7	-0.091717	41.8
64	2s ² 7p	² P ^o _{1/2}	186745.9	-0.090387		-0.090313	
65	2s ² 7p	² P ^o _{3/2}	186746.3	-0.090383	0.4	-0.090302	1.1
66	2s ² 7d	² D ^e _{3/2}	187353	-0.084854		-0.084804	
67	2s ² 7d	² D ^e _{5/2}	187353	-0.084854	0.0	-0.084764	4.4
68	2s ² 7f	² F ^o _{5/2}	187641.6	-0.082225		-0.082171	
69	2s ² 7f	² F ^o _{7/2}	187641.6	-0.082225	0.0	-0.082171	0.0
70	2s ² 7g	² G ^e _{7/2}	187691.4	-0.081771		-0.081744	
71	2s ² 7g	² G ^e _{9/2}	187691.4	-0.081771	0.0	-0.081744	0.0
72	2s ² 7h	² H ^o _{9/2}	187701	-0.081683		-0.081645	
73	2s ² 7h	² H ^o _{11/2}	187701	-0.081683	0.0	-0.081645	0.0
74	2s ² 8s	² S ^e _{1/2}	—	—		-0.074324	
75	2s2p(³ P ^o)3p	² D ^e _{3/2}	188581.25	-0.073662		-0.071901	
76	2s2p(³ P ^o)3p	² D ^e _{5/2}	188615.07	-0.073354	33.8	-0.071582	34.9
77	2s ² 8p	² P ^o _{1/2}	—	—		-0.068349	
78	2s ² 8p	² P ^o _{3/2}	—	—		-0.068343	0.7
79	2s ² 8f	² F ^o _{5/2}	—	—		-0.062873	
80	2s ² 8f	² F ^o _{7/2}	—	—		-0.062872	0.0
81	2s ² 8g	² G ^e _{7/2}	189794.2	-0.062609		-0.062580	
82	2s ² 8g	² G ^e _{9/2}	189794.2	-0.062609	0.0	-0.062580	0.0
83	2s ² 8h	² H ^o _{11/2}	—	—		-0.062511	
84	2s ² 8h	² H ^o _{9/2}	—	—		-0.062511	0.0
85	2s ² 8d	² D ^e _{3/2}	—	—		-0.062612	
86	2s ² 8d	² D ^e _{5/2}	—	—		-0.062564	5.3

Table 1 continued.

In.	Config.	Level	NEEW	NEER	FSS	TER	FSSR
87	2s ² 9s	2S ^e _{1/2}	—	—		-0.057638	
88	2s ² 9p	2P ^o _{1/2}	—	—		-0.053490	
89	2s ² 9p	2P ^o _{3/2}	—	—		-0.053486	0.4
90	2s ² 9d	2D ^e _{3/2}	—	—		-0.049942	
91	2s ² 9d	2D ^e _{5/2}	—	—		-0.049935	0.8
92	2s ² 9f	2F ^o _{5/2}	—	—		-0.049651	
93	2s ² 9f	2F ^o _{7/2}	—	—		-0.049650	0.0
94	2s ² 9g	2G ^e _{7/2}	—	—		-0.049441	
95	2s ² 9g	2G ^e _{9/2}	—	—		-0.049441	0.0
96	2s ² 9h	2H ^o _{9/2}	—	—		-0.049392	
97	2s ² 9h	2H ^o _{11/2}	—	—		-0.049392	0.0
98	2s ² 10s	2S ^e _{1/2}	—	—		-0.046050	
99	2s ² 10p	2P ^o _{1/2}	—	—		-0.042990	
100	2s ² 10p	2P ^o _{3/2}	—	—		-0.042987	0.3
101	2s ² 10d	2D ^e _{3/2}	—	—		-0.040487	
102	2s ² 10d	2D ^e _{5/2}	—	—		-0.040484	0.3
103	2s ² 10f	2F ^o _{5/2}	—	—		-0.040198	
104	2s ² 10f	2F ^o _{7/2}	—	—		-0.040198	0.0
105	2s ² 10g	2G ^e _{7/2}	—	—		-0.040044	
106	2s ² 10g	2G ^e _{9/2}	—	—		-0.040044	0.0
107	2s ² 10h	2H ^o _{9/2}	—	—		-0.040007	
108	2s ² 10h	2H ^o _{11/2}	—	—		-0.040007	0.0
109	2s ² 11s	2S ^e _{1/2}	—	—		-0.037746	
110	2s ² 11p	2P ^o _{1/2}	—	—		-0.035300	
111	2s ² 11p	2P ^o _{3/2}	—	—		-0.035298	0.2
112	2s ² 11d	2D ^e _{3/2}	—	—		-0.033449	
113	2s ² 11d	2D ^e _{5/2}	—	—		-0.033448	0.2
114	2s ² 11f	2F ^o _{5/2}	—	—		-0.033209	
115	2s ² 11f	2F ^o _{7/2}	—	—		-0.033209	0.0
116	2s ² 11g	2G ^e _{7/2}	—	—		-0.033092	
117	2s ² 11g	2G ^e _{9/2}	—	—		-0.033092	0.0
118	2s ² 11h	2H ^o _{9/2}	—	—		-0.033064	
119	2s ² 11h	2H ^o _{11/2}	—	—		-0.033064	0.0
120	2s ² 12s	2S ^e _{1/2}	—	—		-0.031953	
121	2s ² 12p	2P ^o _{1/2}	—	—		-0.029501	
122	2s ² 12p	2P ^o _{3/2}	—	—		-0.029499	0.2
123	2s2p(³ P ^o)3p	2S ^e _{1/2}	—	—		-0.028972	
124	2s ² 12d	2D ^e _{3/2}	—	—		-0.028090	
125	2s ² 12d	2D ^e _{5/2}	—	—		-0.028089	0.1
126	2s ² 12f	2F ^o _{5/2}	—	—		-0.027895	
127	2s ² 12f	2F ^o _{7/2}	—	—		-0.027895	0.0
128	2s ² 12g	2G ^e _{7/2}	—	—		-0.027804	
129	2s ² 12g	2G ^e _{9/2}	—	—		-0.027804	0.0

Table 1 continued.

In.	Config.	Level	NEEW	NEER	FSS	TER	FSSR
130	2s ² 12h	2H ^o _{9/2}	—	—		-0.027783	
131	2s ² 12h	2H ^o _{11/2}	—	—		-0.027783	0.0
132	2s ² 13s	2S ^e _{1/2}	—	—		-0.025758	
133	2s ² 13p	2P ^o _{1/2}	—	—		-0.025021	
134	2s ² 13p	2P ^o _{3/2}	—	—		-0.025020	0.1
135	2s ² 13d	2D ^e _{3/2}	—	—		-0.023920	
136	2s ² 13d	2D ^e _{5/2}	—	—		-0.023919	0.1
137	2s ² 13f	2F ^o _{5/2}	—	—		-0.023762	
138	2s ² 13f	2F ^o _{7/2}	—	—		-0.023762	0.0
139	2s ² 13g	2G ^e _{7/2}	—	—		-0.023690	
140	2s ² 13g	2G ^e _{9/2}	—	—		-0.023690	0.0
141	2s ² 13h	2H ^o _{9/2}	—	—		-0.023673	
142	2s ² 13h	2H ^o _{11/2}	—	—		-0.023673	0.0
143	2s2p(³ P ^o)3d	4F ^o _{3/2}	195752.58	-0.008312			
144	2s2p(³ P ^o)3d	4F ^o _{5/2}	195765.85	-0.008191			
145	2s2p(³ P ^o)3d	4F ^o _{7/2}	195785.74	-0.008010			
146	2s2p(³ P ^o)3d	4F ^o _{9/2}	195813.66	-0.007755	61.1		
147	2s2p(³ P ^o)3d	4D ^o _{1/2}	196557.87	-0.000974			
148	2s2p(³ P ^o)3d	4D ^o _{3/2}	196563.41	-0.000923			
149	2s2p(³ P ^o)3d	4D ^o _{5/2}	196571.82	-0.000846			
150	2s2p(³ P ^o)3d	4D ^o _{7/2}	196581.96	-0.000754	24.1		

^a Index.

^b Configuration. The 1s² core is suppressed from all configurations.

^c NIST Experimental Energy in Wavenumbers (cm⁻¹) relative to the ground state.

^d NIST Experimental Energy in Rydberg relative to the C²⁺ 1S₀^e limit.

^e Fine Structure Splitting from experimental values in cm⁻¹.

^f Theoretical Energy in Rydberg from **R**-matrix calculations relative to the C²⁺ 1S₀^e limit.

^g Fine Structure Splitting from **R**-matrix in cm⁻¹. The minus sign indicates that the theoretical levels are in reverse order compared to the experimental.

Table 2

The available experimental data from NIST for the resonance states of C^+ above the $C^{2+} 1S_0^e$ threshold alongside the theoretical results as obtained by **K**-matrix and **QB** methods.

In. ^a	Config. ^b	Level	NEEW ^c	NEER ^d	FSS ^e	TERK ^f	FSSK ^g	FWHMK ^h	TERQ ⁱ	FSSQ ^j	FWHMQ ^k
1	2s2p(³ P ^o)3d	² D _{3/2} ^o	198425.43	0.016045		0.017012		6.00E-10	0.017012		6.00E-10
2	2s2p(³ P ^o)3d	² D _{5/2} ^o	198436.31	0.016144	10.9	0.017124	12.3	2.61E-09	0.017124	12.3	2.61E-09
3	2s2p(³ P ^o)3d	⁴ P _{5/2} ^o	198844	0.019859		0.020655		2.17E-11	—		—
4	2s2p(³ P ^o)3d	⁴ P _{3/2} ^o	198865.25	0.020053		0.020849		1.26E-09	0.020849		1.26E-09
5	2s2p(³ P ^o)3d	⁴ P _{1/2} ^o	198879.01	0.020178	35.0	0.020968	34.3	5.10E-10	0.020968		5.10E-10
6	2s2p(³ P ^o)3d	² F _{5/2} ^o	199941.41	0.029860		0.031693		5.61E-05	0.031689		5.61E-05
7	2s2p(³ P ^o)3d	² F _{7/2} ^o	199983.24	0.030241	41.8	0.032109	45.6	5.79E-05	0.032106	45.8	5.79E-05
8	2s2p(³ P ^o)3d	² P _{3/2} ^o	202179.85	0.050258		0.053787		1.06E-05	0.053787		1.06E-05
9	2s2p(³ P ^o)3d	² P _{1/2} ^o	202204.52	0.050483	24.7	0.054019	25.5	1.12E-05	0.054019	25.5	1.12E-05
10	2s2p(³ P ^o)4s	⁴ P _{1/2} ^o	209552.36	0.117441		0.118682		2.55E-07	0.118682		2.55E-07
11	2s2p(³ P ^o)4s	⁴ P _{3/2} ^o	209576.46	0.117661		0.118938		6.25E-07	0.118938		6.25E-07
12	2s2p(³ P ^o)4s	⁴ P _{5/2} ^o	209622.32	0.118079	70.0	0.119304	68.3	<1.0E-16	—		—
13	2s2p(³ P ^o)4s	² P _{1/2} ^o	—	—		0.137883		6.13E-03	0.137866		6.02E-03
14	2s2p(³ P ^o)4s	² P _{3/2} ^o	—	—		0.138385	55.0	6.15E-03	0.138365	54.8	6.03E-03
15	2s2p(³ P ^o)4p	² P _{1/2} ^e	214404.33	0.161655		0.162743		2.12E-08	0.162743		2.12E-08
16	2s2p(³ P ^o)4p	² P _{3/2} ^e	214429.95	0.161889	25.6	0.162996	27.7	9.89E-08	0.162996	27.8	9.89E-08
17	2s2p(³ P ^o)4p	⁴ D _{1/2} ^e	214759.91	0.164896		0.165629		5.30E-11	0.165629		5.31E-11
18	2s2p(³ P ^o)4p	⁴ D _{3/2} ^e	214772.84	0.165014		0.165760		5.12E-08	0.165760		5.12E-08
19	2s2p(³ P ^o)4p	⁴ D _{5/2} ^e	214795.27	0.165218		0.165984		6.95E-08	0.165984		6.95E-08
20	2s2p(³ P ^o)4p	⁴ D _{7/2} ^e	214829.77	0.165532	69.9	—	—	—	—	—	—
21	2s2p(³ P ^o)4p	⁴ S _{3/2} ^e	215767.77	0.174080		0.174625		6.59E-12	—		—
22	2s2p(³ P ^o)4p	⁴ P _{1/2} ^e	216362.84	0.179503		0.180780		7.26E-08	0.180780		7.26E-08
23	2s2p(³ P ^o)4p	⁴ P _{3/2} ^e	216379.59	0.179655		0.180931		1.03E-07	0.180931		1.03E-07
24	2s2p(³ P ^o)4p	⁴ P _{5/2} ^e	216400.57	0.179846	37.7	0.181145	40.0	6.05E-07	0.181145	40.0	6.05E-07
25	2s2p(³ P ^o)4p	² D _{3/2} ^e	—	—		0.185420		1.19E-03	0.185422		1.18E-03
26	2s2p(³ P ^o)4p	² D _{5/2} ^e	216927	0.184644		0.185859	48.2	1.18E-03	0.185859	48.0	1.18E-03
27	2s2p(³ P ^o)4p	² S _{1/2} ^e	—	—		0.199765		4.28E-04	0.199765		4.28E-04
28	2s2p(¹ P ^o)3s	² P _{1/2} ^o	—	—		0.205892		3.03E-03	0.205889		3.02E-03
29	2s2p(¹ P ^o)3s	² P _{3/2} ^o	—	—		0.205912	2.2	3.01E-03	0.205909	2.2	3.01E-03
30	2s2p(³ P ^o)4d	⁴ F _{3/2} ^o	219556.54	0.208606		0.208824		5.08E-11	0.208824		5.08E-11
31	2s2p(³ P ^o)4d	⁴ F _{5/2} ^o	219570.15	0.208730		0.208968		4.23E-09	0.208968		4.23E-09
32	2s2p(³ P ^o)4d	⁴ F _{7/2} ^o	219590.76	0.208918		0.209174		5.96E-09	0.209174		5.96E-09
33	2s2p(³ P ^o)4d	⁴ F _{9/2} ^o	219619.88	0.209183	63.3	—	—	—	—	—	—
34	2s2p(³ P ^o)4d	⁴ D _{1/2} ^o	220125.51	0.213791		0.214804		2.31E-09	0.214804		2.31E-09
35	2s2p(³ P ^o)4d	⁴ D _{3/2} ^o	220130.86	0.213839		0.214847		1.06E-09	0.214847		1.06E-09
36	2s2p(³ P ^o)4d	⁴ D _{5/2} ^o	220139.41	0.213917		0.214923		1.33E-09	0.214923		1.33E-09
37	2s2p(³ P ^o)4d	⁴ D _{7/2} ^o	220150.49	0.214018	25.0	0.215042	26.1	6.19E-09	0.215042	26.1	6.19E-09
38	2s2p(³ P ^o)4d	² D _{3/2} ^o	220601.53	0.218128		0.219325		1.99E-08	0.219325		1.99E-08
39	2s2p(³ P ^o)4d	² D _{5/2} ^o	220614.51	0.218247	13.0	0.219441	12.7	5.68E-09	0.219441	12.7	5.68E-09
40	2s2p(³ P ^o)4d	⁴ P _{5/2} ^o	220811.69	0.220044		0.220495		2.43E-10	0.220495		2.43E-10
41	2s2p(³ P ^o)4d	⁴ P _{3/2} ^o	220832.15	0.220230		0.220680		5.32E-10	0.220680		5.32E-10
42	2s2p(³ P ^o)4d	⁴ P _{1/2} ^o	220845.07	0.220348	33.4	0.220796	33.0	3.65E-10	0.220796	33.0	3.65E-10

Table 2 continued.

In.	Config.	Level	NEEW	NEER	FSS	TERK	FSSK	FWHMK	TERQ	FSSQ	FWHMQ
43	2s2p(³ P ^o)4f	² F _{5/2} ^e	221088.88	0.222570		0.223542		9.13E-09	0.223542		9.13E-09
44	2s2p(³ P ^o)4f	² F _{7/2} ^e	221097.92	0.222652	9.0	0.223626	9.2	1.98E-11	—		—
45	2s2p(³ P ^o)4f	⁴ F _{3/2} ^e	221093.95	0.222616		0.223626		5.96E-09	0.223626		5.96E-09
46	2s2p(³ P ^o)4f	⁴ F _{5/2} ^e	221099.11	0.222663		0.223658		5.90E-09	0.223658		5.90E-09
47	2s2p(³ P ^o)4f	⁴ F _{7/2} ^e	221105.73	0.222723		0.223725		5.43E-10	0.223725		5.43E-10
48	2s2p(³ P ^o)4f	⁴ F _{9/2} ^e	221109.78	0.222760	15.8	0.223779	16.8	1.26E-09	0.223779	16.8	1.26E-09
49	2s2p(³ P ^o)4d	² F _{5/2} ^o	221460.88	0.225959		0.227144		1.45E-05	0.227144		1.45E-05
50	2s2p(³ P ^o)4d	² F _{7/2} ^o	221503.33	0.226346	42.4	0.227556	45.1	1.51E-05	0.227556	45.1	1.51E-05
51	2s2p(³ P ^o)4f	⁴ G _{5/2} ^e	221544.81	0.226724		0.227648		5.45E-10	0.227648		5.46E-10
52	2s2p(³ P ^o)4f	⁴ G _{7/2} ^e	221553.99	0.226808		0.227757		7.22E-09	0.227757		7.22E-09
53	2s2p(³ P ^o)4f	⁴ G _{9/2} ^e	221575.61	0.227005		0.227966		6.53E-09	0.227966		6.54E-09
54	2s2p(³ P ^o)4f	⁴ G _{11/2} ^e	221604.9	0.227272	60.1	—		—	—		—
55	2s2p(³ P ^o)4f	² G _{7/2} ^e	221587.12	0.227110		0.228164		2.58E-08	0.228164		2.58E-08
56	2s2p(³ P ^o)4f	² G _{9/2} ^e	221625.72	0.227462	38.6	0.228541	41.4	4.16E-08	0.228541	41.4	4.16E-08
57	2s2p(³ P ^o)4f	⁴ D _{7/2} ^e	221698.48	0.228125		0.229105		2.97E-12	—		—
58	2s2p(³ P ^o)4f	⁴ D _{5/2} ^e	221707.71	0.228209		0.229229		2.39E-06	0.229229		2.39E-06
59	2s2p(³ P ^o)4f	⁴ D _{3/2} ^e	221729.69	0.228409		0.229418		7.35E-07	0.229418		7.35E-07
60	2s2p(³ P ^o)4f	⁴ D _{1/2} ^e	221742.79	0.228528	44.3	0.229529	46.5	<1.0E-16	—		—
61	2s2p(³ P ^o)4f	² D _{5/2} ^e	221729.92	0.228411		0.229459		4.77E-06	0.229459		4.77E-06
62	2s2p(³ P ^o)4f	² D _{3/2} ^e	221752.26	0.228615	22.3	0.229695	25.9	6.58E-06	0.229696	25.9	6.58E-06
63	2s2p(³ P ^o)4d	² P _{3/2} ^o	222258.8	0.233231		0.234626		2.42E-05	0.234626		2.42E-05
64	2s2p(³ P ^o)4d	² P _{1/2} ^o	222285.7	0.233476	26.9	0.234870	26.8	2.46E-05	0.234870	26.8	2.46E-05

^a Index.

^b Configuration. The 1s² core is suppressed from all configurations.

^c NIST Experimental Energy in Wavenumbers (cm⁻¹) relative to the ground state.

^d NIST Experimental Energy in Rydberg relative to the C²⁺ ¹S₀^e limit.

^e Fine Structure Splitting from experimental values in cm⁻¹.

^f Theoretical Energy in Rydberg from **K**-matrix calculations relative to the C²⁺ ¹S₀^e limit.

^g Fine Structure Splitting from **K**-matrix in cm⁻¹.

^h Full Width at Half Maximum from **K**-matrix in Rydberg.

ⁱ Theoretical Energy in Rydberg from **QB** calculations relative to the C²⁺ ¹S₀^e limit.

^j Fine Structure Splitting from **QB** in cm⁻¹.

^k Full Width at Half Maximum from **QB** in Rydberg.

Table 3

Free-bound f -values for bound symmetry $J^\pi = 1/2^o$ obtained by integrating photoionization cross sections from **R**-matrix calculations. The superscript denotes the power of 10 by which the number is to be multiplied.

In.	1	12	20	22	27	32	34	49	64	77	88	99	110	121	133
15	6.12^{-3}	1.57^{-3}	5.60^{-4}	4.58^{-5}	1.92^{-2}	1.01^{-3}	2.89^{-2}	3.93^{-3}	1.55^{-3}	8.99^{-4}	5.98^{-4}	4.26^{-4}	3.17^{-4}	2.44^{-4}	1.92^{-4}
16	3.18^{-3}	8.30^{-4}	2.69^{-4}	1.21^{-5}	9.72^{-3}	5.02^{-4}	1.47^{-2}	2.02^{-3}	7.92^{-4}	4.63^{-4}	3.07^{-4}	2.20^{-4}	1.64^{-4}	1.26^{-4}	9.93^{-5}
17	1.70^{-5}	4.69^{-6}	1.59^{-6}	1.34^{-2}	5.91^{-5}	2.92^{-6}	8.14^{-5}	1.09^{-5}	4.27^{-6}	2.47^{-6}	1.64^{-6}	1.16^{-6}	8.63^{-7}	6.60^{-7}	5.15^{-7}
18	8.53^{-6}	3.43^{-6}	4.94^{-7}	1.35^{-2}	1.19^{-5}	7.05^{-7}	2.68^{-5}	5.00^{-6}	1.95^{-6}	1.19^{-6}	8.00^{-7}	5.89^{-7}	4.64^{-7}	3.50^{-7}	2.90^{-7}
21	4.43^{-7}	1.39^{-7}	5.34^{-8}	1.78^{-3}	1.67^{-6}	7.21^{-8}	2.04^{-6}	2.71^{-7}	1.04^{-7}	5.92^{-8}	3.88^{-8}	2.71^{-8}	1.99^{-8}	1.51^{-8}	1.18^{-8}
22	4.48^{-7}	3.87^{-7}	4.64^{-9}	2.22^{-4}	6.57^{-13}	7.26^{-8}	8.82^{-7}	1.54^{-7}	7.90^{-8}	5.31^{-8}	3.85^{-8}	2.95^{-8}	2.41^{-8}	1.91^{-8}	1.53^{-8}
23	2.44^{-6}	1.65^{-6}	6.16^{-7}	1.01^{-3}	1.65^{-7}	5.61^{-8}	7.62^{-7}	5.76^{-7}	3.75^{-7}	2.74^{-7}	2.08^{-7}	1.61^{-7}	1.27^{-7}	1.02^{-7}	8.32^{-8}
25	1.81^{-2}	1.13^{-2}	3.63^{-3}	3.44^{-7}	2.22^{-3}	1.01^{-3}	1.66^{-2}	7.00^{-3}	4.20^{-3}	2.96^{-3}	2.20^{-3}	1.69^{-3}	1.32^{-3}	1.05^{-3}	8.50^{-4}
27	1.81^{-3}	2.76^{-3}	7.42^{-4}	3.83^{-8}	1.55^{-3}	4.26^{-4}	2.16^{-3}	4.12^{-4}	2.69^{-4}	1.98^{-4}	1.52^{-4}	1.20^{-4}	9.55^{-5}	7.73^{-5}	6.32^{-5}
45	1.31^{-9}	3.51^{-8}	1.80^{-8}	7.18^{-7}	3.61^{-6}	6.21^{-6}	1.84^{-5}	6.64^{-7}	1.40^{-7}	6.59^{-8}	4.25^{-8}	2.98^{-8}	2.26^{-8}	1.82^{-8}	1.53^{-8}
59	8.42^{-7}	3.47^{-6}	1.84^{-6}	6.24^{-4}	4.20^{-4}	6.82^{-4}	1.99^{-3}	6.74^{-5}	1.46^{-5}	6.42^{-6}	3.64^{-6}	2.34^{-6}	1.61^{-6}	1.17^{-6}	8.82^{-7}
60	1.93^{-10}	1.70^{-10}	2.09^{-11}	5.12^{-4}	1.07^{-9}	1.51^{-9}	3.28^{-9}	2.78^{-10}	7.52^{-13}	2.96^{-13}	2.36^{-13}	1.88^{-13}	5.71^{-13}	4.68^{-13}	3.86^{-13}
62	8.30^{-6}	1.94^{-5}	1.09^{-5}	6.60^{-5}	3.76^{-3}	6.16^{-3}	1.74^{-2}	5.94^{-4}	1.29^{-4}	5.62^{-5}	3.17^{-5}	2.03^{-5}	1.39^{-5}	1.00^{-5}	7.51^{-6}

Table 4

Free-bound f -values for bound symmetry $J^\pi = 3/2^\circ$ obtained by integrating photoionization cross sections from **R**-matrix calculations. The superscript denotes the power of 10 by which the number is to be multiplied.

In.	2	13	14	18	21	23	28	33	35	50	65	78	89	100	111	122	134
15	1.49 ⁻³	3.73 ⁻⁴	3.75 ⁻¹⁰	2.32 ⁻³	1.45 ⁻⁴	6.09 ⁻⁶	4.82 ⁻³	2.45 ⁻⁴	7.17 ⁻³	9.78 ⁻⁴	3.82 ⁻⁴	2.21 ⁻⁴	1.47 ⁻⁴	1.04 ⁻⁴	7.77 ⁻⁵	5.97 ⁻⁵	4.69 ⁻⁵
16	7.53 ⁻³	1.91 ⁻³	1.58 ⁻⁹	4.40 ⁻⁴	7.03 ⁻⁴	2.70 ⁻⁵	2.39 ⁻²	1.23 ⁻³	3.60 ⁻²	4.91 ⁻³	1.92 ⁻³	1.11 ⁻³	7.36 ⁻⁴	5.25 ⁻⁴	3.91 ⁻⁴	2.99 ⁻⁴	2.35 ⁻⁴
17	4.15 ⁻⁶	1.12 ⁻⁶	1.96 ⁻¹⁰	6.73 ⁻⁶	4.15 ⁻⁷	1.33 ⁻³	1.48 ⁻⁵	7.06 ⁻⁷	2.02 ⁻⁵	2.73 ⁻⁶	1.06 ⁻⁶	6.09 ⁻⁷	4.02 ⁻⁷	2.85 ⁻⁷	2.11 ⁻⁷	1.61 ⁻⁷	1.26 ⁻⁷
18	9.38 ⁻⁶	2.33 ⁻⁶	1.26 ⁻⁹	2.57 ⁻⁷	9.49 ⁻⁷	8.54 ⁻³	3.96 ⁻⁵	1.87 ⁻⁶	5.00 ⁻⁵	6.55 ⁻⁶	2.40 ⁻⁶	1.38 ⁻⁶	9.09 ⁻⁷	6.43 ⁻⁷	4.53 ⁻⁷	3.45 ⁻⁷	2.68 ⁻⁷
19	8.52 ⁻⁷	6.35 ⁻⁷	2.88 ⁻⁹	1.31 ⁻⁸	6.29 ⁻⁸	1.70 ⁻²	3.61 ⁻⁷	1.17 ⁻⁷	4.99 ⁻⁷	4.47 ⁻⁷	2.97 ⁻⁷	2.18 ⁻⁷	1.67 ⁻⁷	1.30 ⁻⁷	1.03 ⁻⁷	8.24 ⁻⁸	6.72 ⁻⁸
21	1.07 ⁻⁶	3.31 ⁻⁷	9.71 ⁻⁹	7.28 ⁻⁸	1.41 ⁻⁷	1.73 ⁻³	4.13 ⁻⁶	1.77 ⁻⁷	5.05 ⁻⁶	6.70 ⁻⁷	2.56 ⁻⁷	1.45 ⁻⁷	9.47 ⁻⁸	6.65 ⁻⁸	4.88 ⁻⁸	3.70 ⁻⁸	2.88 ⁻⁸
22	8.46 ⁻⁸	1.94 ⁻⁷	3.34 ⁻⁶	2.59 ⁻⁸	8.10 ⁻⁸	6.20 ⁻⁴	5.42 ⁻⁷	5.30 ⁻⁸	2.18 ⁻⁸	3.66 ⁻⁸	3.16 ⁻⁸	2.63 ⁻⁸	2.16 ⁻⁸	1.76 ⁻⁸	1.44 ⁻⁸	1.18 ⁻⁸	8.36 ⁻⁹
23	8.05 ⁻⁷	3.16 ⁻⁷	6.69 ⁻⁶	3.12 ⁻⁷	7.82 ⁻⁸	1.75 ⁻⁴	8.71 ⁻⁷	5.77 ⁻⁸	1.69 ⁻⁶	3.10 ⁻⁷	1.41 ⁻⁷	8.84 ⁻⁸	6.13 ⁻⁸	4.48 ⁻⁸	3.38 ⁻⁸	2.61 ⁻⁸	2.06 ⁻⁸
24	1.21 ⁻⁵	7.19 ⁻⁶	1.02 ⁻⁵	1.33 ⁻⁷	1.97 ⁻⁶	5.70 ⁻⁴	1.39 ⁻⁶	9.26 ⁻⁷	9.35 ⁻⁶	4.66 ⁻⁶	2.71 ⁻⁶	1.93 ⁻⁶	1.44 ⁻⁶	1.11 ⁻⁶	8.68 ⁻⁷	6.92 ⁻⁷	5.60 ⁻⁷
25	2.17 ⁻³	1.34 ⁻³	4.07 ⁻¹⁰	2.32 ⁻³	3.60 ⁻⁴	1.03 ⁻⁷	2.82 ⁻⁴	1.55 ⁻⁴	1.81 ⁻³	7.25 ⁻⁴	4.35 ⁻⁴	3.06 ⁻⁴	2.27 ⁻⁴	1.74 ⁻⁴	1.36 ⁻⁴	1.08 ⁻⁴	8.72 ⁻⁵
26	1.65 ⁻²	1.03 ⁻²	7.75 ⁻⁹	2.52 ⁻⁴	2.85 ⁻³	1.34 ⁻⁶	2.04 ⁻³	6.47 ⁻⁴	1.55 ⁻²	6.42 ⁻³	3.82 ⁻³	2.70 ⁻³	2.01 ⁻³	1.40 ⁻³	1.10 ⁻³	8.74 ⁻⁴	7.06 ⁻⁴
27	1.83 ⁻³	2.69 ⁻³	5.75 ⁻⁹	3.73 ⁻⁸	6.92 ⁻⁴	9.90 ⁻⁸	1.46 ⁻³	4.33 ⁻⁴	2.26 ⁻³	4.40 ⁻⁴	2.77 ⁻⁴	2.29 ⁻⁴	1.76 ⁻⁴	1.39 ⁻⁴	1.11 ⁻⁴	8.97 ⁻⁵	7.34 ⁻⁵
43	8.82 ⁻¹⁰	3.29 ⁻⁸	2.11 ⁻¹¹	1.95 ⁻²	4.70 ⁻¹⁰	3.85 ⁻⁷	4.71 ⁻⁶	9.11 ⁻⁶	2.73 ⁻⁵	9.58 ⁻⁷	2.10 ⁻⁷	9.16 ⁻⁸	5.05 ⁻⁸	3.29 ⁻⁸	2.22 ⁻⁸	1.56 ⁻⁸	1.13 ⁻⁸
45	1.40 ⁻¹⁰	3.21 ⁻⁹	1.02 ⁻¹³	1.56 ⁻⁶	1.28 ⁻⁹	4.30 ⁻⁷	3.43 ⁻⁷	5.82 ⁻⁷	1.77 ⁻⁶	6.67 ⁻⁸	1.43 ⁻⁸	7.03 ⁻⁹	4.33 ⁻⁹	3.03 ⁻⁹	2.30 ⁻⁹	1.85 ⁻⁹	1.55 ⁻⁹
46	3.92 ⁻¹⁰	1.91 ⁻⁸	3.10 ⁻¹²	8.73 ⁻⁴	9.29 ⁻⁹	1.59 ⁻⁶	3.18 ⁻⁶	5.65 ⁻⁶	1.69 ⁻⁵	5.77 ⁻⁷	1.32 ⁻⁷	6.04 ⁻⁸	3.58 ⁻⁸	2.41 ⁻⁸	1.77 ⁻⁸	1.37 ⁻⁸	1.11 ⁻⁸
51	2.59 ⁻¹⁰	2.29 ⁻⁹	4.10 ⁻¹³	2.84 ⁻⁵	1.02 ⁻⁹	2.51 ⁻⁸	2.90 ⁻⁷	4.87 ⁻⁷	1.41 ⁻⁶	4.77 ⁻⁸	1.03 ⁻⁸	4.54 ⁻⁹	2.56 ⁻⁹	1.64 ⁻⁹	1.13 ⁻⁹	8.19 ⁻¹⁰	6.15 ⁻¹⁰
58	2.89 ⁻⁶	9.08 ⁻⁶	8.44 ⁻¹⁰	3.22 ⁻⁵	3.81 ⁻⁶	5.82 ⁻⁴	1.25 ⁻³	2.06 ⁻³	5.93 ⁻³	1.97 ⁻⁴	4.20 ⁻⁵	1.81 ⁻⁵	1.05 ⁻⁵	6.70 ⁻⁶	4.61 ⁻⁶	3.32 ⁻⁶	2.49 ⁻⁶
59	7.73 ⁻⁹	3.06 ⁻⁷	2.55 ⁻¹¹	1.70 ⁻⁴	1.65 ⁻⁷	3.98 ⁻⁴	4.12 ⁻⁵	6.90 ⁻⁵	1.98 ⁻⁴	6.91 ⁻⁶	1.45 ⁻⁶	6.29 ⁻⁷	3.54 ⁻⁷	2.39 ⁻⁷	1.64 ⁻⁷	1.19 ⁻⁷	8.89 ⁻⁸
60	1.58 ⁻¹¹	1.07 ⁻¹²	1.03 ⁻¹⁰	3.51 ⁻¹¹	9.86 ⁻¹²	5.14 ⁻⁵	2.41 ⁻¹⁰	3.99 ⁻¹⁰	8.16 ⁻¹⁰	1.11 ⁻¹⁰	6.77 ⁻¹³	5.32 ⁻¹³	4.18 ⁻¹³	3.31 ⁻¹³	3.03 ⁻¹³	2.46 ⁻¹³	2.00 ⁻¹³
61	6.45 ⁻⁶	1.47 ⁻⁵	5.74 ⁻⁹	2.85 ⁻⁵	7.05 ⁻⁶	2.76 ⁻⁴	2.50 ⁻³	4.03 ⁻³	1.17 ⁻²	4.03 ⁻⁴	8.49 ⁻⁵	3.67 ⁻⁵	2.07 ⁻⁵	1.31 ⁻⁵	8.95 ⁻⁶	6.41 ⁻⁶	4.77 ⁻⁶
62	6.54 ⁻⁷	1.93 ⁻⁶	8.56 ⁻¹⁰	1.53 ⁻³	1.60 ⁻⁶	4.23 ⁻⁵	3.67 ⁻⁴	5.87 ⁻⁴	1.70 ⁻³	6.05 ⁻⁵	1.31 ⁻⁵	5.72 ⁻⁶	3.24 ⁻⁶	2.07 ⁻⁶	1.42 ⁻⁶	1.02 ⁻⁶	7.67 ⁻⁷

Table 5

Free-bound f -values for bound symmetry $J^\pi = 5/2^\circ$ obtained by integrating photoionization cross sections from **R**-matrix calculations. The superscript denotes the power of 10 by which the number is to be multiplied.

In.	17	24	29	38	53	68	79	92	103	114	126	137
16	2.78^{-3}	2.11^{-7}	1.34^{-8}	8.88^{-9}	8.79^{-9}	8.27^{-9}	7.47^{-9}	6.57^{-9}	5.69^{-9}	4.90^{-9}	4.15^{-9}	3.61^{-9}
18	4.47^{-6}	5.27^{-4}	3.69^{-9}	3.39^{-9}	3.30^{-9}	3.25^{-9}	3.14^{-9}	3.18^{-9}	3.12^{-9}	3.09^{-9}	2.98^{-9}	3.21^{-9}
19	1.24^{-7}	4.78^{-3}	4.64^{-10}	4.43^{-10}	4.37^{-10}	4.30^{-10}	4.17^{-10}	4.00^{-10}	3.82^{-10}	3.48^{-10}	3.66^{-10}	3.99^{-10}
20	2.32^{-9}	1.20^{-2}	1.72^{-17}	1.38^{-16}	3.10^{-15}	0	0	0	0	0	0	0
21	4.56^{-7}	1.61^{-3}	3.64^{-13}	3.65^{-13}	3.21^{-13}	1.59^{-13}	1.15^{-13}	4.49^{-15}	7.60^{-14}	7.09^{-14}	7.56^{-14}	1.44^{-13}
23	2.24^{-8}	5.24^{-4}	9.47^{-9}	8.94^{-9}	9.08^{-9}	8.40^{-9}	6.36^{-9}	5.54^{-9}	4.76^{-9}	4.07^{-9}	3.93^{-9}	3.43^{-9}
24	1.24^{-6}	1.07^{-3}	3.20^{-9}	2.91^{-9}	2.67^{-9}	2.43^{-9}	2.17^{-9}	1.92^{-9}	1.69^{-9}	1.48^{-9}	1.30^{-9}	1.14^{-9}
25	1.57^{-4}	1.52^{-10}	5.59^{-5}	4.91^{-5}	3.89^{-5}	3.48^{-5}	3.05^{-5}	2.63^{-5}	2.26^{-5}	1.93^{-5}	1.65^{-5}	1.25^{-5}
26	2.29^{-3}	3.79^{-8}	3.50^{-6}	3.16^{-6}	2.83^{-6}	2.51^{-6}	2.20^{-6}	1.90^{-6}	1.63^{-6}	1.39^{-6}	1.19^{-6}	9.00^{-7}
43	8.17^{-4}	1.17^{-7}	3.26^{-7}	5.10^{-7}	6.46^{-7}	7.25^{-7}	7.59^{-7}	7.58^{-7}	7.35^{-7}	6.97^{-7}	6.51^{-7}	6.02^{-7}
44	1.46^{-2}	2.83^{-6}	9.13^{-8}	7.43^{-8}	9.39^{-8}	1.06^{-7}	1.12^{-7}	1.14^{-7}	1.12^{-7}	1.08^{-7}	1.03^{-7}	9.68^{-8}
45	1.09^{-7}	2.81^{-8}	1.63^{-8}	2.04^{-10}	2.08^{-10}	2.01^{-10}	1.94^{-10}	1.87^{-10}	1.83^{-10}	1.98^{-10}	2.20^{-10}	2.44^{-10}
46	2.49^{-5}	4.66^{-7}	3.70^{-9}	2.17^{-8}	2.74^{-8}	3.06^{-8}	3.17^{-8}	3.13^{-8}	2.99^{-8}	2.77^{-8}	2.50^{-8}	2.22^{-8}
47	4.70^{-3}	9.64^{-7}	4.28^{-8}	9.19^{-9}	1.03^{-8}	1.06^{-8}	1.05^{-8}	9.61^{-9}	8.45^{-9}	7.13^{-9}	5.78^{-9}	4.46^{-9}
51	5.49^{-7}	7.39^{-9}	1.91^{-8}	2.24^{-10}	2.40^{-10}	2.20^{-10}	1.69^{-10}	1.04^{-10}	4.31^{-11}	4.57^{-12}	1.03^{-11}	9.47^{-11}
52	3.19^{-7}	1.35^{-7}	2.87^{-7}	7.10^{-7}	9.12^{-7}	1.04^{-6}	1.11^{-6}	1.13^{-6}	1.12^{-6}	1.09^{-6}	1.04^{-6}	9.99^{-7}
55	5.58^{-5}	6.96^{-8}	3.70^{-6}	5.17^{-6}	6.57^{-6}	7.40^{-6}	7.76^{-6}	7.76^{-6}	7.51^{-6}	7.11^{-6}	6.62^{-6}	6.08^{-6}
57	1.23^{-5}	9.69^{-4}	1.91^{-9}	3.11^{-10}	4.07^{-10}	4.68^{-10}	5.02^{-10}	5.15^{-10}	5.15^{-10}	5.06^{-10}	4.92^{-10}	4.75^{-10}
58	6.08^{-4}	1.62^{-4}	1.33^{-8}	5.77^{-9}	5.26^{-9}	4.56^{-9}	3.83^{-9}	3.16^{-9}	2.57^{-9}	2.10^{-9}	1.70^{-9}	1.41^{-9}
59	1.27^{-5}	2.48^{-5}	8.56^{-9}	2.70^{-8}	2.53^{-8}	2.30^{-8}	2.04^{-8}	1.77^{-8}	1.52^{-8}	1.31^{-8}	1.11^{-8}	9.56^{-9}
61	1.26^{-3}	8.08^{-5}	1.74^{-9}	4.53^{-9}	3.89^{-9}	3.29^{-9}	2.76^{-9}	2.31^{-9}	1.95^{-9}	1.65^{-9}	1.41^{-9}	1.24^{-9}
62	1.12^{-4}	2.75^{-6}	2.04^{-7}	2.38^{-7}	2.25^{-7}	2.05^{-7}	1.81^{-7}	1.57^{-7}	1.36^{-7}	1.17^{-7}	9.93^{-8}	8.59^{-8}

Table 6

Sample of our line list where several lines have been observed astronomically. The first column is for experimental/theoretical energy identification for the upper and lower states respectively where 1 refers to experimental while 0 refers to theoretical. The other columns are for the atomic designation of the upper and lower states respectively, followed by the air wavelength in angstrom and effective dielectronic recombination rate coefficients in cm^3s^{-1} for the given logarithmic temperatures. The superscript denotes the power of 10 by which the number is to be multiplied.

ET	Upper	Lower	λ_{air}	$\log_{10}(T)$						
				2.0	2.5	3.0	3.5	4.0	4.5	
11	2s2p(³ P ^o)4f ⁴ D ^e _{1/2}	2s2p(³ P ^o)3d ² P ^o _{1/2}	5116.73	5.53 ⁻¹⁹⁰	2.59 ⁻⁸¹	1.85 ⁻⁴⁷	2.89 ⁻³⁷	1.48 ⁻³⁴	3.27 ⁻³⁴	
11	2s2p(³ P ^o)4f ⁴ D ^e _{5/2}	2s2p(³ P ^o)3d ² P ^o _{3/2}	5119.46	5.14 ⁻¹⁶⁸	9.10 ⁻⁶²	1.11 ⁻²⁸	9.88 ⁻¹⁹	4.25 ⁻¹⁶	8.88 ⁻¹⁶	
11	2s2p(³ P ^o)3p ² P ^e _{3/2}	2s ² 4p ² P ^o _{1/2}	5120.08	2.50 ⁻²⁶	1.64 ⁻¹⁹	7.84 ⁻¹⁸	3.26 ⁻¹⁷	3.79 ⁻¹⁷	1.76 ⁻¹⁷	
11	2s2p(³ P ^o)4f ⁴ D ^e _{3/2}	2s2p(³ P ^o)3d ² P ^o _{1/2}	5120.17	6.88 ⁻¹⁶⁹	1.51 ⁻⁶²	1.97 ⁻²⁹	1.80 ⁻¹⁹	7.78 ⁻¹⁷	1.63 ⁻¹⁶	
11	2s2p(³ P ^o)3p ² P ^e _{3/2}	2s ² 4p ² P ^o _{3/2}	5121.83	1.20 ⁻²⁵	7.87 ⁻¹⁹	3.75 ⁻¹⁷	1.56 ⁻¹⁶	1.81 ⁻¹⁶	8.40 ⁻¹⁷	
11	2s ² 7f ² F ^o _{5/2}	2s ² 4d ² D ^e _{3/2}	5122.09	6.05 ⁻²⁹	7.95 ⁻²²	2.03 ⁻¹⁸	9.32 ⁻¹⁸	6.66 ⁻¹⁸	3.55 ⁻¹⁸	
11	2s ² 7f ² F ^o _{7/2}	2s ² 4d ² D ^e _{5/2}	5122.27	2.11 ⁻²⁸	1.95 ⁻²¹	3.05 ⁻¹⁸	1.44 ⁻¹⁷	1.03 ⁻¹⁷	5.43 ⁻¹⁸	
11	2s ² 7f ² F ^o _{5/2}	2s ² 4d ² D ^e _{5/2}	5122.27	4.32 ⁻³⁰	5.68 ⁻²³	1.45 ⁻¹⁹	6.66 ⁻¹⁹	4.76 ⁻¹⁹	2.54 ⁻¹⁹	
11	2s2p(³ P ^o)3p ² P ^e _{1/2}	2s ² 4p ² P ^o _{1/2}	5125.21	1.46 ⁻²⁶	8.64 ⁻²⁰	4.82 ⁻¹⁸	5.15 ⁻¹⁷	7.05 ⁻¹⁷	3.50 ⁻¹⁷	
11	2s2p(³ P ^o)3p ² P ^e _{1/2}	2s ² 4p ² P ^o _{3/2}	5126.96	7.08 ⁻²⁷	4.20 ⁻²⁰	2.34 ⁻¹⁸	2.50 ⁻¹⁷	3.42 ⁻¹⁷	1.70 ⁻¹⁷	
11	2s2p(³ P ^o)3p ⁴ P ^e _{3/2}	2s2p(³ P ^o)3s ⁴ P ^o _{1/2}	5132.95	4.96 ⁻²⁸	9.80 ⁻²⁰	1.65 ⁻¹⁷	2.49 ⁻¹⁶	2.26 ⁻¹⁵	1.48 ⁻¹⁵	
11	2s2p(³ P ^o)3p ⁴ P ^e _{5/2}	2s2p(³ P ^o)3s ⁴ P ^o _{3/2}	5133.28	1.69 ⁻²⁷	1.09 ⁻¹⁹	1.71 ⁻¹⁷	1.66 ⁻¹⁶	1.50 ⁻¹⁵	1.08 ⁻¹⁵	
11	2s2p(³ P ^o)3p ⁴ P ^e _{1/2}	2s2p(³ P ^o)3s ⁴ P ^o _{1/2}	5137.26	1.15 ⁻²⁸	5.07 ⁻²⁰	8.50 ⁻¹⁸	9.92 ⁻¹⁷	8.62 ⁻¹⁶	5.55 ⁻¹⁶	
11	2s2p(³ P ^o)3p ⁴ P ^e _{3/2}	2s2p(³ P ^o)3s ⁴ P ^o _{3/2}	5139.17	1.57 ⁻²⁸	3.10 ⁻²⁰	5.23 ⁻¹⁸	7.89 ⁻¹⁷	7.15 ⁻¹⁶	4.68 ⁻¹⁶	
01	2s ² 11p ² P ^o _{3/2}	2s ² 5s ² S ^e _{1/2}	5141.70	9.29 ⁻³³	1.36 ⁻²⁵	3.26 ⁻²¹	1.25 ⁻¹⁹	6.35 ⁻¹⁹	6.92 ⁻¹⁹	
01	2s ² 11p ² P ^o _{1/2}	2s ² 5s ² S ^e _{1/2}	5141.76	2.10 ⁻³³	4.79 ⁻²⁶	1.60 ⁻²¹	6.26 ⁻²⁰	3.16 ⁻¹⁹	3.48 ⁻¹⁹	
11	2s2p(³ P ^o)3p ⁴ P ^e _{1/2}	2s2p(³ P ^o)3s ⁴ P ^o _{3/2}	5143.49	5.77 ⁻²⁸	2.55 ⁻¹⁹	4.27 ⁻¹⁷	4.99 ⁻¹⁶	4.34 ⁻¹⁵	2.79 ⁻¹⁵	
11	2s2p(³ P ^o)3p ⁴ P ^e _{5/2}	2s2p(³ P ^o)3s ⁴ P ^o _{5/2}	5145.16	3.97 ⁻²⁷	2.56 ⁻¹⁹	4.01 ⁻¹⁷	3.90 ⁻¹⁶	3.54 ⁻¹⁵	2.53 ⁻¹⁵	
11	2s2p(³ P ^o)3p ⁴ P ^e _{3/2}	2s2p(³ P ^o)3s ⁴ P ^o _{5/2}	5151.08	5.59 ⁻²⁸	1.11 ⁻¹⁹	1.86 ⁻¹⁷	2.81 ⁻¹⁶	2.55 ⁻¹⁵	1.67 ⁻¹⁵	
11	2s2p(³ P ^o)4f ⁴ G ^e _{5/2}	2s2p(³ P ^o)3d ² P ^o _{3/2}	5162.53	1.92 ⁻¹⁷¹	6.83 ⁻⁶⁶	5.01 ⁻³³	3.80 ⁻²³	1.56 ⁻²⁰	3.20 ⁻²⁰	
11	2s2p(³ P ^o)3d ² D ^o _{5/2}	2s ² 5g ² G ^e _{7/2}	5162.98	7.68 ⁻³³	5.07 ⁻²⁶	2.23 ⁻²⁴	2.27 ⁻²⁴	7.55 ⁻²⁵	2.38 ⁻²⁵	
00	2s2p(³ P ^o)4s ² P ^o _{3/2}	2s ² 11s ² S ^e _{1/2}	5172.37	8.25 ⁻¹⁰⁸	1.12 ⁻⁴³	6.57 ⁻²⁴	3.60 ⁻¹⁸	7.20 ⁻¹⁷	5.71 ⁻¹⁷	
00	2s2p(³ P ^o)4s ² P ^o _{1/2}	2s ² 11s ² S ^e _{1/2}	5187.14	9.10 ⁻¹⁰⁸	7.19 ⁻⁴⁴	3.55 ⁻²⁴	1.84 ⁻¹⁸	3.63 ⁻¹⁷	2.86 ⁻¹⁷	
10	2s2p(³ P ^o)4s ⁴ P ^o _{3/2}	2s ² 9s ² S ^e _{1/2}	5196.92	7.54 ⁻⁹⁸	1.97 ⁻⁴³	9.74 ⁻²⁷	5.69 ⁻²²	5.63 ⁻²¹	3.57 ⁻²¹	
10	2s2p(³ P ^o)4s ⁴ P ^o _{1/2}	2s ² 9s ² S ^e _{1/2}	5203.44	1.74 ⁻⁹⁸	3.58 ⁻⁴⁴	1.65 ⁻²⁷	9.41 ⁻²³	9.23 ⁻²²	5.84 ⁻²²	
11	2s2p(³ P ^o)3p ⁴ D ^e _{5/2}	2s ² 4p ² P ^o _{3/2}	5203.77	7.63 ⁻³³	2.44 ⁻²⁴	4.07 ⁻²²	7.12 ⁻²¹	1.35 ⁻¹⁹	1.71 ⁻¹⁹	
11	2s2p(³ P ^o)4p ⁴ S ^e _{3/2}	2s2p(³ P ^o)3d ⁴ D ^o _{1/2}	5204.20	2.74 ⁻¹³⁷	2.03 ⁻⁵⁶	2.33 ⁻³¹	6.55 ⁻²⁴	5.86 ⁻²²	8.17 ⁻²²	
11	2s2p(³ P ^o)4p ⁴ S ^e _{3/2}	2s2p(³ P ^o)3d ⁴ D ^o _{3/2}	5205.70	1.73 ⁻¹³⁶	1.28 ⁻⁵⁵	1.48 ⁻³⁰	4.15 ⁻²³	3.71 ⁻²¹	5.18 ⁻²¹	
11	2s2p(³ P ^o)4p ⁴ S ^e _{3/2}	2s2p(³ P ^o)3d ⁴ D ^o _{5/2}	5207.98	3.34 ⁻¹³⁶	2.47 ⁻⁵⁵	2.84 ⁻³⁰	8.00 ⁻²³	7.15 ⁻²¹	9.98 ⁻²¹	
11	2s2p(³ P ^o)3p ⁴ D ^e _{3/2}	2s ² 4p ² P ^o _{1/2}	5208.74	1.87 ⁻³¹	3.80 ⁻²⁴	4.99 ⁻²²	1.05 ⁻²⁰	1.62 ⁻¹⁹	1.83 ⁻¹⁹	
11	2s2p(³ P ^o)3p ⁴ D ^e _{3/2}	2s ² 4p ² P ^o _{3/2}	5210.56	2.50 ⁻³⁰	5.10 ⁻²³	6.70 ⁻²¹	1.41 ⁻¹⁹	2.17 ⁻¹⁸	2.46 ⁻¹⁸	
11	2s2p(³ P ^o)3p ⁴ D ^e _{1/2}	2s ² 4p ² P ^o _{1/2}	5212.65	1.15 ⁻³⁰	2.43 ⁻²³	3.42 ⁻²¹	1.01 ⁻¹⁹	1.06 ⁻¹⁸	8.41 ⁻¹⁹	
11	2s2p(³ P ^o)3p ⁴ D ^e _{1/2}	2s ² 4p ² P ^o _{3/2}	5214.46	5.52 ⁻³¹	1.17 ⁻²³	1.64 ⁻²¹	4.85 ⁻²⁰	5.09 ⁻¹⁹	4.03 ⁻¹⁹	
11	2s2p(³ P ^o)4p ⁴ D ^e _{7/2}	2s2p(³ P ^o)3d ⁴ F ^o _{5/2}	5244.05	1.17 ⁻¹⁵⁸	1.89 ⁻⁶¹	3.48 ⁻³¹	4.16 ⁻²²	9.58 ⁻²⁰	1.65 ⁻¹⁹	
11	2s2p(³ P ^o)4p ⁴ D ^e _{7/2}	2s2p(³ P ^o)3d ⁴ F ^o _{7/2}	5249.53	2.53 ⁻¹⁵⁷	4.08 ⁻⁶⁰	7.50 ⁻³⁰	8.98 ⁻²¹	2.07 ⁻¹⁸	3.55 ⁻¹⁸	
11	2s2p(³ P ^o)4p ⁴ D ^e _{5/2}	2s2p(³ P ^o)3d ⁴ F ^o _{3/2}	5249.90	1.29 ⁻¹²⁶	6.68 ⁻⁵⁰	3.73 ⁻²⁶	3.70 ⁻¹⁹	1.86 ⁻¹⁷	1.97 ⁻¹⁷	
11	2s2p(³ P ^o)4p ⁴ D ^e _{5/2}	2s2p(³ P ^o)3d ⁴ F ^o _{5/2}	5253.56	2.49 ⁻¹²⁵	1.29 ⁻⁴⁸	7.20 ⁻²⁵	7.15 ⁻¹⁸	3.59 ⁻¹⁶	3.80 ⁻¹⁶	
11	2s2p(³ P ^o)4p ⁴ D ^e _{3/2}	2s2p(³ P ^o)3d ⁴ F ^o _{3/2}	5256.09	2.63 ⁻¹²⁵	1.09 ⁻⁴⁸	5.69 ⁻²⁵	5.52 ⁻¹⁸	2.75 ⁻¹⁶	2.91 ⁻¹⁶	
11	2s2p(³ P ^o)4p ⁴ D ^e _{7/2}	2s2p(³ P ^o)3d ⁴ F ^o _{9/2}	5257.24	2.45 ⁻¹⁵⁶	3.96 ⁻⁵⁹	7.27 ⁻²⁹	8.71 ⁻²⁰	2.01 ⁻¹⁷	3.44 ⁻¹⁷	
11	2s2p(³ P ^o)4p ⁴ D ^e _{5/2}	2s2p(³ P ^o)3d ⁴ F ^o _{7/2}	5259.06	1.26 ⁻¹²⁴	6.53 ⁻⁴⁸	3.64 ⁻²⁴	3.61 ⁻¹⁷	1.81 ⁻¹⁵	1.92 ⁻¹⁵	
11	2s2p(³ P ^o)4p ⁴ D ^e _{1/2}	2s2p(³ P ^o)3d ⁴ F ^o _{3/2}	5259.66	1.46 ⁻¹²⁶	5.35 ⁻⁵⁰	2.67 ⁻²⁶	2.65 ⁻¹⁹	1.51 ⁻¹⁷	1.78 ⁻¹⁷	